

A Histological Study on Platelet Poor Plasma versus Platelet Rich Plasma in Amelioration of Induced Diabetic Neuropathy in Rats and the Potential Role of Telocyte-like Cells

Dalia Ibrahim Ismail and Eman Abas Farag

Department of Histology, Faculty of Medicine, Cairo University, Egypt

ABSTRACT

Background: Diabetic neuropathy (DN) is a major chronic diabetes complication characterized by functional and structural alterations in peripheral nerves. Platelet rich plasma (PRP) is an encouraged biological blood derivative that has gained publicity in diverse applications and proved its efficacy.

Aim of Work: Evaluate the probable ameliorating effect of platelet poor plasma (PPP) versus PRP on induced DN in rats.

Materials and Methods: This study included 48 male adult albino rats, 10 to obtain PRP and PPP. Thirty eight were divided into 4 groups; group I (control). Group II (DN group): received a single intraperitoneal STZ (60 mg/kg) injection and were left till the end of the experiment. Groups III (PRP group) and IV (PPP group) received subcutaneous PRP or PPP 0.5 mL/kg, 2 times a week for 3 weeks after 60 days diabetes. Body weight, blood glucose and miR-146a and nerve conduction velocity (NCV) were assessed, as well as tissue MDA, TNF α , NGF, ZO-1 and claudin-1. Right sciatic nerve specimens were taken and processed for HandE, toluidine blue stains, S100, CD34 and caspase-3 immunohistochemical stains and TEM. Number of CD34 immunopositive cells and area percent of S100 and caspase-3 immunoreaction were measured, in addition to G-ratio and capillary luminal area. This was followed by statistical analysis.

Results: DN group showed altered biochemical and histological features; axonopathy, Schwannopathy and angiopathy, with affected NCV and telocyte-like cells (TLCs). PRP and PPP groups showed comparable results to each other and to the control. They revealed almost normal biochemical and histological features and NCV. In addition, they revealed significant increase in S100 and CD34 immunoexpression with significant decrease in area percent of caspase-3 versus DN group.

Conclusion: PPP and PRP proved to exert ameliorative effect on DN through improving the biochemical and histopathological alterations and TLCs preservation.

Received: 15 April 2020, Accepted: 23 April 2020

Key Words: Diabetic Neuropathy; PPP; PRP; Schwann cells; Telocyte-like Cells.

Corresponding Author: Dalia Ibrahim Ismail, MD, Department of Histology, Faculty of Medicine, Cairo University, Egypt, Tel.: +20 1005050870, **E-mail:** drdaliaibrahim@hotmail.com

ISSN: 1110-0559, Vol. 44, No.1

INTRODUCTION

The worldwide prevalence of diabetic neuropathy (DN) reaches up to 30% of diabetic patients; about 66% of type 1 as well as about 59% of type 2 own the tendency to develop neuropathy. It is one of the least understood and most debilitating and difficult to treat complication of diabetes mellitus (DM). It leads to ulceration, gangrene or even amputations^[1]. Even though, therapies targeting DN are hindered by its complexity and the poor knowledge about its diverse causes^[2]. Yet there are two hypotheses; the metabolic one that proposed elevated oxidative stress (OS) resulting in mitochondrial malfunction, glycosylation of protein in addition to inflammation^[3], and the vascular hypothesis where there are microangiopathy and neurovascular changes that reduce glucose and oxygen extracted by nerve cells^[4]. Both hypotheses could be applied but not restricted and probably interact for the occurrence and advancement of DN^[2].

To reverse DN deficits, an essential strategy is the activation of intrinsic neurotrophic pathways; as its

pathogenesis involves degeneration and deficient regeneration due to the unsupportive microenvironment around axons resulting from microangiopathy and ischemia, Schwann cells (SCs) dysfunction, altered basement membranes, impaired macrophage clearance and lack of growth factors (GFs)s. Thus adding GFs is potentially an essential approach to achieve regeneration^[5]. Blood platelets contain copious growth and neurotrophic factors that are released once activated and attract cells to damaged areas, increase their mitotic activity and angiogenesis^[6,7]. Administration of GFs in the form of PRP is the way; it is a cheap, easily obtained and with no hazards of immune reaction or rejection being autologous^[8]. That is why plasma preparations, PRP and lately PPP, have revealed plentiful advantages and hopeful curative standpoints^[9].

Peripheral nerves consist of axons with their defensive SCs enclosed within layers of connective tissues; epineurium, perineurium and endoneurium. Schwann cells and endoneurial endothelial cells (ECs) alongside the

particular perineurial sheath assure nerve homeostasis^[10]. Schwann cells are concerned with the basic aspects of nerve biology; as conduction of impulses, production of extracellular matrix, plus trophic support for nerve cells and their regeneration^[11]. Apoptosis of SCs and ECs disturbs nerves' microenvironment and function leading to neuronal loss^[12]. Also, tight junctions (TJs) are critical for maintaining nerve normal function; acting as defensive and diffusion barrier for endoneurial microenvironment and among these are zonula occludens-1 (ZO-1), claudins and occludin. Zonula occludens-1 is a cytoplasmic TJs associated protein organizing their composition and determining claudins polymerization. Claudin-1 is the most prominent member of claudin family, found mainly in the perineurium and endoneurial vessels, and plays a crucial role in maintaining blood nerve barrier (BNB). It was reported that ZO-1 and claudin-1 expressions are modified during nerve injury^[2,10].

Telocytes (TCs) are particular interstitial cells occupying a strategic position in the stroma of many tissues and organs; near or in contact with capillaries and peripheral nerves and around stem cell niche, which is correlated with their capability to create homo- and hetero-cellular contacts (3D network) in addition to the extracellular release of microvesicles, suggesting a special role in cell signaling. Also their tactical location makes them an attractive field for research and provides opportunities for clinical applications in regenerative medicine. Somewhat endoneurial dendritic cells might be assimilated to TCs or, at least, considered a particular cell phenotype, namely telocyte-like cells (TLCs). The ultrastructural characteristics using TEM remains the golden way to exactly identify TCs; so far there is no single specific immunomarker for their detection, yet CD34 is recently accepted as a reliable TCs marker^[13].

MicroRNAs (miRNAs) are non-coding small RNAs mediating RNA interference by post-transcription modulation of gene expression and protein synthesis; so involved in several developmental, physiological and pathological processes. Lately, miRNAs gained an increasing interest for their additional roles as diagnostic tests in several diseases because of their easy detection and stability in serum. Moreover, recent studies have proposed that miRNAs might be involved in DN even if their role in its onset and development is not fully understood^[14,15].

Platelet rich plasma has been the topic in different studies, however no histological study was done to target the influence of PRP on experimentally-induced DN and also no study used PPP in this issue. That is why this study was established to investigate the ameliorating effect of PPP versus PRP on DN in albino rat model of DM. As well investigating the possible mechanisms by which PPP and PRP could induce their effects.

MATERIALS AND METHODS

Streptozotocin

It was provided as a vial containing 1 gm active streptozotocin (STZ) powder, freshly prepared using citrate

buffer (0.1 mol/L and pH 4.5); so each rat received 0.5 mL of intraperitoneal (IP) citrate buffer containing 12 mg STZ^[16]. Both were purchased from Sigma Aldrich, St. Louis, Missouri, USA.

Animals

Forty eight adult male albino rats were included, with average weight (180- 200 grams) and about 3 months old. They were housed under standard environmental conditions in the Animal House, Faculty of Medicine, with free entry to standard diet and water. All the experimental procedures were carried out in accordance with the rules of Cairo University Animal Use Committee.

Experimental design

Ten rats from the 48 were used for obtaining PPP and PRP; using autologous plasma is technically impossible as small animals do not have adequate blood, whilst the other 38 were divided randomly into:

- Group I (Control group): 8 rats were equally subdivided into:
 - Subgroup IA: were left without any intervention.
 - Subgroup IB: fasted overnight then received a single injection of citrate buffer (0.5 mL, IP) and left till the end of the experiment.
 - Subgroup IC: rats treated as subgroup IB then received PRP 0.5 mL/kg subcutaneously twice per week for the last 3 weeks.
 - Subgroup ID: rats managed as subgroup IB and then received 0.5 mL/kg PPP as in subgroup 1C.
- Group II (Diabetic Neuropathy, DN group): 10 rats, fasted overnight, received STZ (60 mg/kg, IP) single injection. Blood samples were taken 72 h after STZ from the tail veins and rats with fasting glucose levels of 250 mg/dl or more were considered diabetic. They were left for 60 days after DM confirmation^[16] and then were left with no intervention for 3 weeks (till the end of the experiment).
- Group III (PRP group): 10 rats dealt with as group II and after 60 days from DM induction, they received subcutaneous injection of PRP in a dose of 0.5 mL/kg two times weekly for additional 3 weeks^[17].
- Group IV (PPP group): 10 rats treated as group II, then after 60 days from induction of DM, they were given PPP subcutaneously in a similar dose and regimen to group III^[17].

Experimental procedure

Body weight measurement

Body weights were recorded for all rats at the beginning of experiment, 60 days after DM confirmation and just before scarification.

Preparation of PRP and PPP

Rats were deeply anaesthetized and under complete aseptic conditions 8-10 mL blood was taken by cardiac puncture into heparinized tubes and centrifuged twice. Firstly, for 10 minutes at 1600 rotation per minute (rpm) resulting in 3 different layers; the inferior was the red blood corpuscles, the middle was the buffy coat of white blood cells. The superior was the plasma that was taken by a pipette without disturbing the buffy coat and centrifuged again for 10 minutes at 2000 rpm. This resulted in 2 fractions; the top is the PPP and underneath is the platelet button. Some of the PPP was collected to be used and part was left with platelet button that was lightly disturbed, to confirm platelets re-suspension and produce PRP. To be certain with platelets concentration, PRP sample was counted automatically to verify platelet count above 1,000,000/ μ L^[18]. Both PPP and PRP were kept frozen and activated immediately before use with 10% CaCl₂ (8mL plasma: 2mL CaCl₂)^[19].

Nerve conduction velocity measurement

After 60 days of DM and by the end of the experiment, rats were anaesthetized with pentobarbital (40 mg/Kg). Proximal and distal ends of the right lower limb were disinfected and fine needle electrodes were inserted in the sciatic notch and ankle. The electrodes were connected to PowerLab 4/25 (AD Instruments, Dunedin, New Zealand) and Bio AMP Amplifier (Castle Hill, Australia). Sciatic nerves were stimulated using square wave pulses (duration= 0.1 ms) with raising intensity to reach the maximum compound action potential (CAP). Then the distance between the electrodes is divided by the latent period (time between applying stimulus and the peak of CAP)^[20]. This was accomplished in Physiology Department, Faculty of Medicine, Cairo University.

Biochemical investigations

After 60 days of DM, samples of blood were taken in heparinized tubes from tail veins for measuring serum miR-146a by quantitative PCR to confirm DN^[14]. At the end of experiment, just before scarification and after overnight fasting, blood samples were taken by the same way to measure blood glucose and serum miR-146a. Rats were sacrificed by pentobarbital (80 mg/Kg, IP)^[21]. From the superior angle of the popliteal fossa, specimens from the right sciatic nerves were dissected and parts of them were taken for preparing tissue homogenates to measure:

- Malondialdehyde (MDA)^[22].
- Tumor necrosis factor alpha (TNF α) using ELISA kits (R&D Systems, Inc.)^[23].
- Nerve growth factor (NGF) using ELISA kits^[1].
- ZO-1 and claudin-1 by western blot analysis^[12].

Preparation of PRP and PPP and biochemical investigations were done in Medical Biochemistry Department, Faculty of Medicine, Cairo University.

Histological studies

Light microscopic study: Sciatic nerve specimens were fixed in 10% formal saline, embedded in paraffin, cut with thickness 6 μ m then stained with:

1. Hematoxylin and eosin (H&E)^[24].
2. Immunohistochemically^[24] using:
 - Anti S100 antibody, a mouse monoclonal antibody (Abcam, MA, USA, ab14849). In neural regeneration research, S100 proteins indicate SCs proliferation^[25].
 - Anti CD34 antibody, a rabbit monoclonal antibody (Abcam, MA, USA, ab81289). CD34 is a marker of hematopoietic stem cells, ECs and TCs as well^[13].
 - Anti caspase-3 antibody, a rabbit polyclonal (Thermo Scientific, CA, USA, PA1-29157).

Transmission electron microscopic (TEM) study: Specimens were cut into 1mm pieces and kept at 4°C overnight in 2.5% glutaraldehyde buffered with phosphate buffer (0.1 mol/L). Then were fixed for 1h in 1% osmium tetroxide and dehydrated via grades of alcohol, embedded in epoxy resin then cut using Leica ultracut (UCT) (Glienicker, Berlin, Germany). Semithin sections (1 μ m) stained with toluidine blue 1% were examined by light microscope. Ultrathin sections (60-90 nm) gathered on copper grids were stained using uranyl acetate and lead citrate^[26] and examined by TEM (JEOL, JEM-1400, Japan) at Electron Microscope Research Unit, Faculty of Agriculture, Cairo University. Telocyte-like cells were digitally colored in blue using Adobe Photoshop 2014 for better visualization.

Morphometric studies

Were performed at Histology Department, Faculty of Medicine, Cairo University by means of Leica Qwin 500 software image analyzer (Leica image system Ltd; Cambridge, England). All were done in 10 non-overlapping fields chosen at random in each section. The following were estimated in semithin sections using x100 oil immersion lens

1. G-ratio (an indicator for nerve function and conduction); diameters of regularly myelinated fibers and their axons were manually measured followed by estimation of axon/fiber ratio^[27].
2. Capillary luminal area represented by the outline of ECs facing the lumen^[28].

The following other parameters were measured in immunostained sections using an objective lens of x40 magnification

1. Area % of S100 immunoreaction.
2. Number of CD34 positive cells in both the endothelium and the interstitium (TLCs & stem cells).
3. Area % of caspase-3 immunoreaction.

Statistical Analysis

Was made for the biochemical and morphometric results. Comparisons between groups were done using ANOVA (analysis of variance) then post hoc Tukey test (SPSS package version 22, SPSS Inc., Chicago, USA). Results were recorded as mean and standard deviation (SD) and considered statistically significant when $p<0.05^{[29]}$.

RESULTS

General Observations

Three rats died throughout the experiment; 2 from group II (DN group) and 1 from group IV (PPP group). The control subgroups presented comparable results so they were named collectively control group.

Body weight, blood glucose and nerve conduction velocity results

These are illustrated in Table 1.

Histological results

Group I (control group)

Nerve sections stained with H&E revealed normal histological architecture of sciatic nerve; nerve bundles were covered by perineurial and epineurial sheathes. Closely packed nerve fibers consisted of faintly stained axons surrounded by unstained myelin and Schwann cells (SCs), with endoneurial blood vessels in between (Figure 1a). In semithin sections, closely packed small and large myelinated and unmyelinated nerve fibers were seen surrounded by perineurial and epineurial sheathes. Myelinated fibers had clear axons surrounded by regular myelin. SCs were enclosing nerve fibers. Endoneurium plus endoneurial blood vessels with flat endothelium and surrounded by pericytes were observed (Figure 1b). S100 immunostained sections revealed profuse positive reaction in the cytoplasm of SCs (Figure 1c). Some CD34 positive ECs and TLCs with their unique telopodes are observed (Figure 1d). Whilst caspase-3 immunoreactivity was not detected (Figure 1e).

Ultrastructurally, the perineurium was formed of several layers of flat perineurial cells with flat euchromatic nuclei, multiple vesicles, mitochondria and surrounded by basal laminae from both sides. Perineurial blood vessels with continuous flat endothelium were seen (Figure 2a). Densely arranged myelinated fibers were formed of axons containing neurotubules, neurofilaments and mitochondria and surrounded by electron dense compact myelin. Some unmyelinated fibers were seen among them. SCs with large euchromatic nuclei and regular continuous basal laminae enclosed both types of fibers (Figures 2b, 2c, 2d). Endoneurial blood vessels with flat continuous endothelium and surrounded by pericytes were also noticed (Figure 2e). Additionally, TLCs with their characteristic telopodes, formed of alternating thin and thick segments, were seen forming a sheath beneath the perineurium and around nerve fibers and endoneurial blood vessels (Figures 2a, 2d, 2e).

Group II (DN group)

Sciatic nerve sections from DN group stained with H&E displayed several bundles, each bounded by irregular perineurial sheath with underlying wide empty space. Marked inflammatory infiltrate was seen among them. Endoneurial and perineurial blood vessels appeared congested and/or collapsed with narrow lumen or with thickened walls. Some apparently normal axons with unstained myelin and SCs were detected. Also areas of degenerated nerve fibers with spacing and some degenerated axons were noticed (Figure 3a). In semithin sections, nerve bundles were enclosed in thickened epineurium wherein macrophages with dark nuclei and vacuolated cytoplasm and mast cells with metachromatically stained granules were seen. These cells were also seen among nerve fibers. Bundles were surrounded by irregular perineurium with underlying empty space. Each bundle had small and large myelinated nerve fibers widely spaced by endoneurium. Many axons appeared retracted and shrunken, surrounded by empty spaces, vacuolated or split myelin and enclosed by SCs. It also revealed congested endoneurial and epineurial blood vessels lined with high ECs and surrounded by thickened and/or interrupted basement membranes that enclosed pericytes (Figures 3b, 3c). Some S100 positivity was detected within SCs (Figure 3d). Few CD34 positive ECs and TLCs were detected (Figure 3e). Whereas, there was abundant positive caspase-3 immunoreaction; in and beneath the perineurium, in the endoneurium and in the endothelium (Figure 3f).

Ultrastructurally, group II sections were covered by perineurium formed of several flat perineurial cells with flat heterochromatic nuclei, multiple vesicles and surrounded by basal laminae from both sides, the perineurium showed underlying widened space (Figure 4a). In the majority of the nerve fibers the axons appeared retracted, surrounded by empty spaces, had vacuolated cytoplasm, degenerated mitochondria and electron dense particles. Additionally, myelin sheathes were markedly vacuolated and split into several layers (Figures 4, 5). Degenerated myelin was fragmented into electron dense myelin debris engulfed by SCs and surrounded by several concentric lamellae formed by SCs processes (onion bulb) (Figure 5a). Moreover, SCs revealed thickened basal laminae, irregular nuclei with more heterochromatin, degenerated mitochondria, dilated rER, vacuolated cytoplasm and large electron dense inclusions (Figure 5a-d). Furthermore, endoneurial blood vessels showed ECs with heterochromatic irregular nuclei, vacuolated cytoplasm and disrupted junctions and surrounded by thickened and/or detached basement membranes. The pericytes were detached from the basement membranes and presented vacuolated cytoplasm, degenerated mitochondria, dilated rER and slightly irregular nuclei with degenerated chromatin and small nucleoli. Some vessels with narrow (collapsed) lumens were also demonstrated (Figures 4b, 4d).

Eosinophils with their bilobed nuclei and characteristic granules, having electron dense crystalline cores surrounded by less electron dense matrix, were detected near the blood vessels (Figure 4b). Mast cells with electron dense

granules, as well as macrophages having kidney shaped nuclei with peripheral heterochromatin, irregular surface showing pseudopodia and vacuolated granular cytoplasm rich in phagosomes and different lysosomes were seen among nerve fibers and in proximity to blood vessels (Figures 4b, 4c). Moreover, there were TLCs with their distinguished telopodes, formed of alternating thin and thick segments, communicating with each other and forming a sheath around nerve fibers and blood vessels. Some of them had large euchromatic nuclei and large vesicles in their cytoplasm and some had small apoptotic nuclei with marked heterochromatin and markedly vacuolated cytoplasm (Figures 4c, 4d, 5c).

Group III (PRP group)

Sections stained with H&E (Figure 6a) and toluidine blue (Figure 6b) and that examined by TEM (Figure 7a-d) showed apparently normal histological features comparable to the control, except for the presence of few areas of degenerated nerve fibers, empty spaces, retracted shrunken axons, small areas of vacuolations in the axons and myelin, electron dense particles and dense inclusions in SCs cytoplasm. Immunohistochemically stained sections revealed profuse S100 positive reaction (Figure 6c). CD34 positive immunoreactivity was detected in the cytoplasm of branched cells with rounded nuclei close to blood vessels; stem cells, ECs and in many TLCs with their telopodes (Figure 6d). Little caspase-3 positive immunoreaction was seen within the endoneurium (Figure 6e).

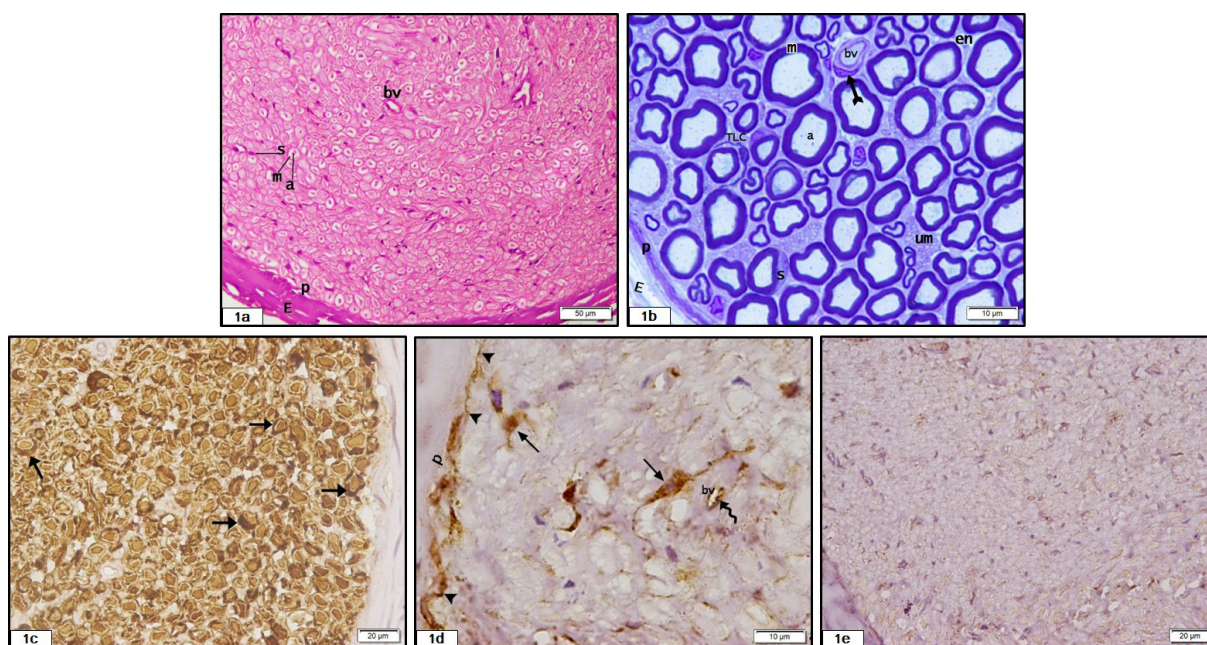


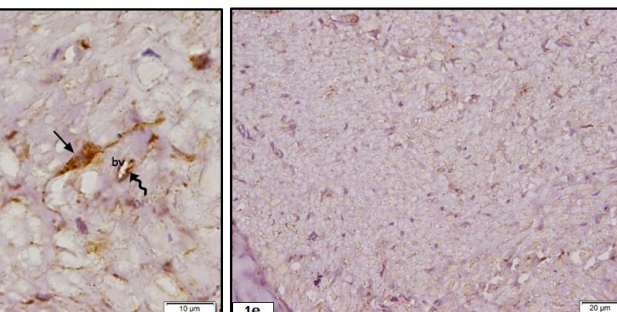
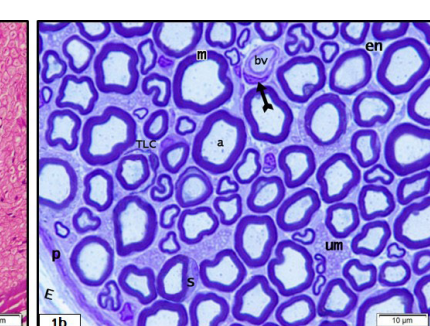
Fig. 1: Photomicrographs of sciatic nerve sections of control group demonstrating: a: Part of nerve bundle with closely packed nerve fibers showing axons (a), unstained myelin (m), nuclei of Schwann cells (S), endoneurial blood vessels (bv) and part of perineurial (P) and epineurial (E) sheathes [H&E, x200]. b: Closely packed small and large myelinated and unmyelinated nerve fibers (um). Myelinated fibers are formed of axons (a) bounded by regular myelin (m). Schwann cells (S) are noticed enclosing nerve fibers. Endoneurium (en), endoneurial blood vessel (bv) with flat endothelium surrounded by pericyte (bifid arrow) and telocyte-like cells (TLC) with their telopodes are observed around nerve fibers. Notice part of perineurial (P) and epineurial (E) sheathes [Toluidine blue, x1000]. c: Abundant S100+ve immunoreaction is seen around axons (arrows) [anti S100 immunohistochemical stain, x400]. d: Some CD34+ve TLCs (arrows) are seen around nerve fibers, with their telopodes (arrow heads) forming sheath beneath the perineurium (P). CD34+ve reaction is seen in endothelial lining (wavy arrow) of blood vessels (bv) [anti CD34 immunohistochemical stain, x1000]. e: Undetectable positive caspase-3 reaction [anti caspase-3 immunohistochemical stain, x400].

Group IV (PPP group)

H&E stained sections (Figure 8a) and semithin sections (Figure 8b) showed improvement in the histological picture comparable to PRP group. Still, there were empty spaces beneath the perineurium and among nerve fibers, which were slightly less packed with areas of degenerated fibers and some degenerated axons. Also, some fibers had retracted shrunken axons, split or invaginated myelin. Few endoneurial blood vessels had high endothelium and partially narrowed lumens. Abundant S100 immunostaining within SCs was seen (Figure 8c). Numerous CD34 positive stem cells, ECs and many TLCs with their telopodes were detected (Figure 8d). There was little positive caspase-3 immunoreaction underneath the perineurium, within the endoneurium and in the endothelium (Figure 8e). Likewise, ultrathin sections displayed fewer morphological alterations when compared to DN group. They showed less obvious axonal and myelin vacuolations and split. Few SCs had degenerated mitochondria and small vacuoles. In addition, some nuclei of TLCs were more heterochromatic. Endoneurial blood vessels were apparently normal but with slightly narrow lumen (Figure 9a-c).

Biochemical and morphometric results

These are illustrated in Table 2.



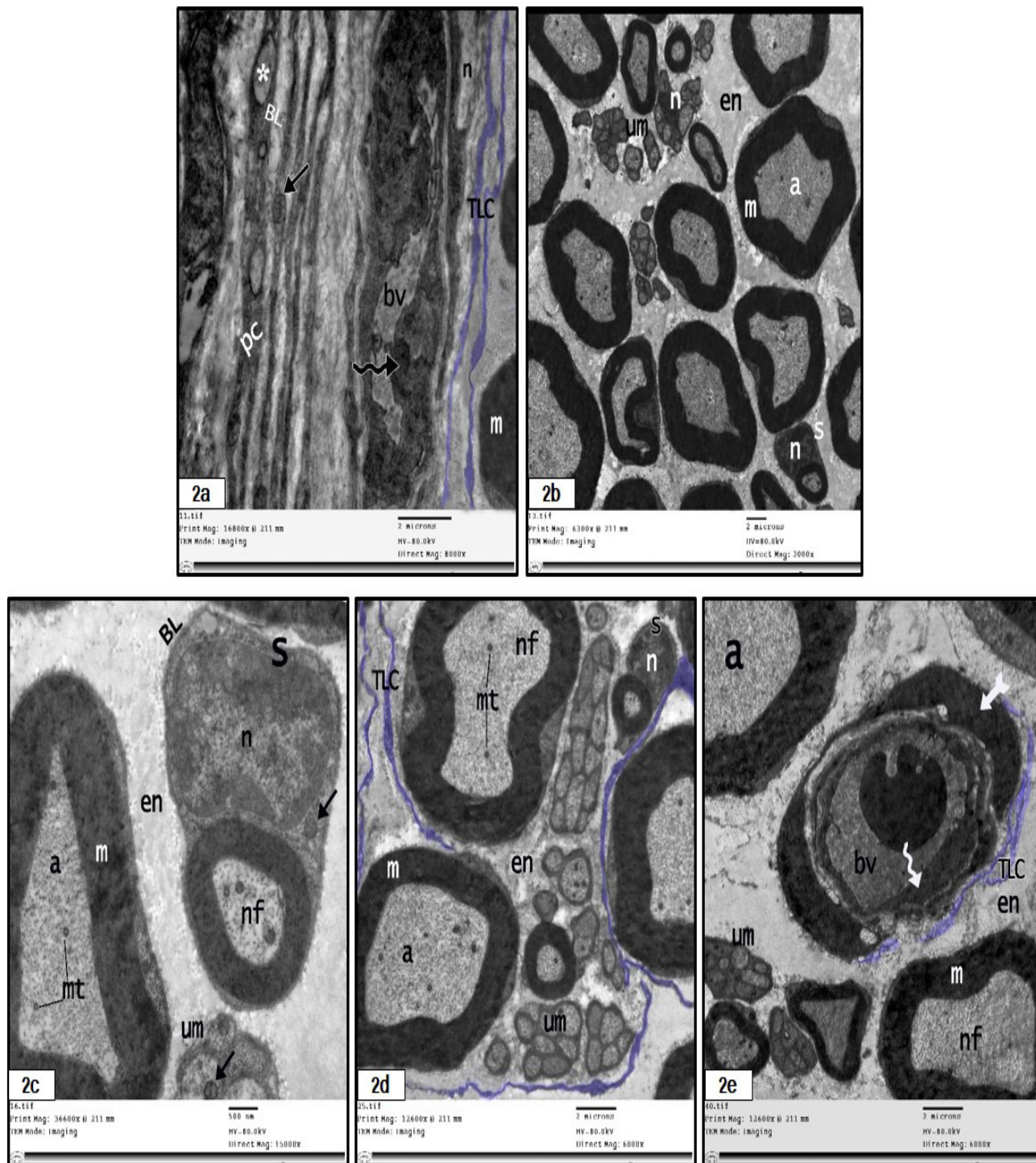


Fig. 2: TEM photomicrographs of sciatic nerve sections from control group showing: a: Part of the perineurium formed of several flat perineurial cells (PC) with flat euchromatic nuclei (n), multiple vesicles (*), mitochondria (arrow) and surrounded by basal laminae (BL). Perineurial blood vessel (bv) with continuous flat endothelium (wavy arrow) is seen. Telopodes of telocyte-like cells (TLC) (digitally colored blue) with alternating thin and thick segments are seen forming sheath beneath the perineurium and around myelinated (m) nerve fibers [x8000]. b: Densely arranged nerve fibers of variable diameters. Myelinated fibers are formed of axons (a) surrounded by electron dense compact myelin (m). Schwann cell (S) and its nucleus (n) are seen enclosing nerve fibers. Endoneurium (en) is seen among the nerve fibers. Notice the presence of unmyelinated fibers (um) [x3000]. c: Higher magnification of the previous figure showing myelinated axons (a), surrounded with compact electron dense myelin sheath (m), and unmyelinated fibers (um) with endoneurium (en) in between. The axoplasm contains neurotubules (mt), neurofilaments (nf) and mitochondria (arrow). A Schwann cell (S) with large euchromatic nucleus (n), regular continuous basal lamina (BL) and mitochondria (arrow) is seen [x15000]. d: Telocyte like cells (TLC) (digitally colored blue) with their telopodes form sheath around myelinated (m) as well as unmyelinated nerve fibers (um). Additionally, Schwann cell (S) with large euchromatic nucleus (n) surrounds myelinated axon (a), also neurotubules (mt), neurofilaments (nf) and endoneurium (en) are observed [x6000]. e: Endoneurial blood vessel (bv) lined with flat continuous endothelium (wavy arrow) is surrounded by pericytes (bifid arrow) and the characteristic telopodes of telocyte like cells (TLC) (digitally colored blue). It also reveals myelinated (m) and unmyelinated (um) axons (a), neurofilaments (nf) and endoneurium (en) [x6000].

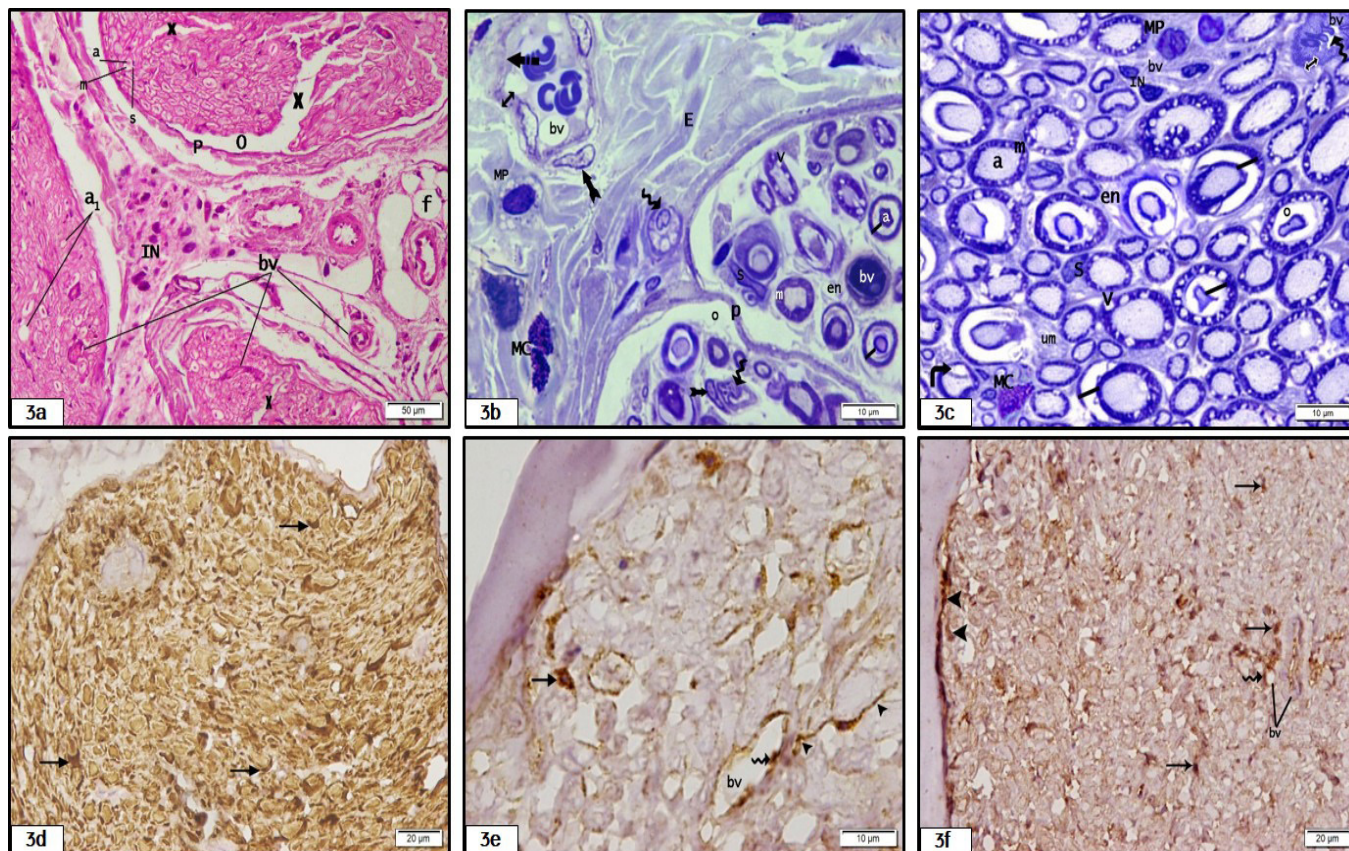


Fig. 3: Photomicrographs of sciatic nerve sections from diabetic group illustrating: a: Three nerve bundles with inflammatory infiltrate (IN) in between; each bundle is enclosed by irregular perineurial sheath (P) with underlying wide empty space (o). Endoneurial and perineurial blood vessels (bv), congested or collapsed or with thickened wall are seen, with the presence of fat cells (f). Axons (a) are surrounded by unstained myelin (m) and nuclei of Schwann cell (S). Areas of degenerated nerve fibers with empty spaces (X) and degenerated axons (a1), are demonstrated [H&E, x200]. b: Two nerve bundles, each is surrounded by irregular perineurium (p) showing wide underlying empty space (O). Bundles are enclosed in thickened epineurium (E), macrophages (MP), with dark nucleus and vacuolated cytoplasm, and mast cells (MC), with metachromatically stained granules, are observed. Each bundle is formed of small and large myelinated nerve fibers spaced out by endoneurium (en). Myelin (m) is seen vacuolated (v) or split (line) around shrunken axons (a). Schwann cells (S) are seen. Congested endoneurial and epineurial blood vessels (bv) lined with high endothelial cells (wavy arrows) are detected, surrounded by thickened (double ended arrow) and interrupted basement membranes (dashed arrow). Pericytes (bifid arrows) are enclosed within the basement membrane [Toluidine blue, x1000]. c: Small and large myelinated and unmyelinated (um) nerve fibers separated by endoneurium (en). Some axons (a) are retracted (right angle arrow) or shrunken surrounded by wide empty space (o). Myelin (m) is seen vacuolated (v) or split (lines) and enclosed by Schwann cells (S). It also reveals congested endoneurial blood vessels (bv) with narrow lumens, lined with high endothelial cells (wavy arrow), surrounded by thickened basement membranes (double ended arrow). There are inflammatory infiltrate (IN), macrophages (MP) with kidney shaped nuclei and mast cell (MC) with metachromatically stained granules [Toluidine blue, x1000]. d: Some S100+ve immunoreaction is seen around axons (arrows) [anti S100 immunohistochemical stain, x 400]. e: Few CD34+ve TLCs (arrow) with their telopodes (arrow heads) are detected around nerve fibers. Also, CD34+ve reaction can be noted in the endothelial lining (wavy arrow) of blood vessels (bv) [anti CD34 immunohistochemical stain, x1000]. f: Abundant caspase-3 +ve reaction is seen in and beneath perineurium (arrow heads), in the endoneurium (arrows) as well as in endothelial lining (wavy arrow) of blood vessels (bv) [anti caspase-3 immunohistochemical stain, x 400].

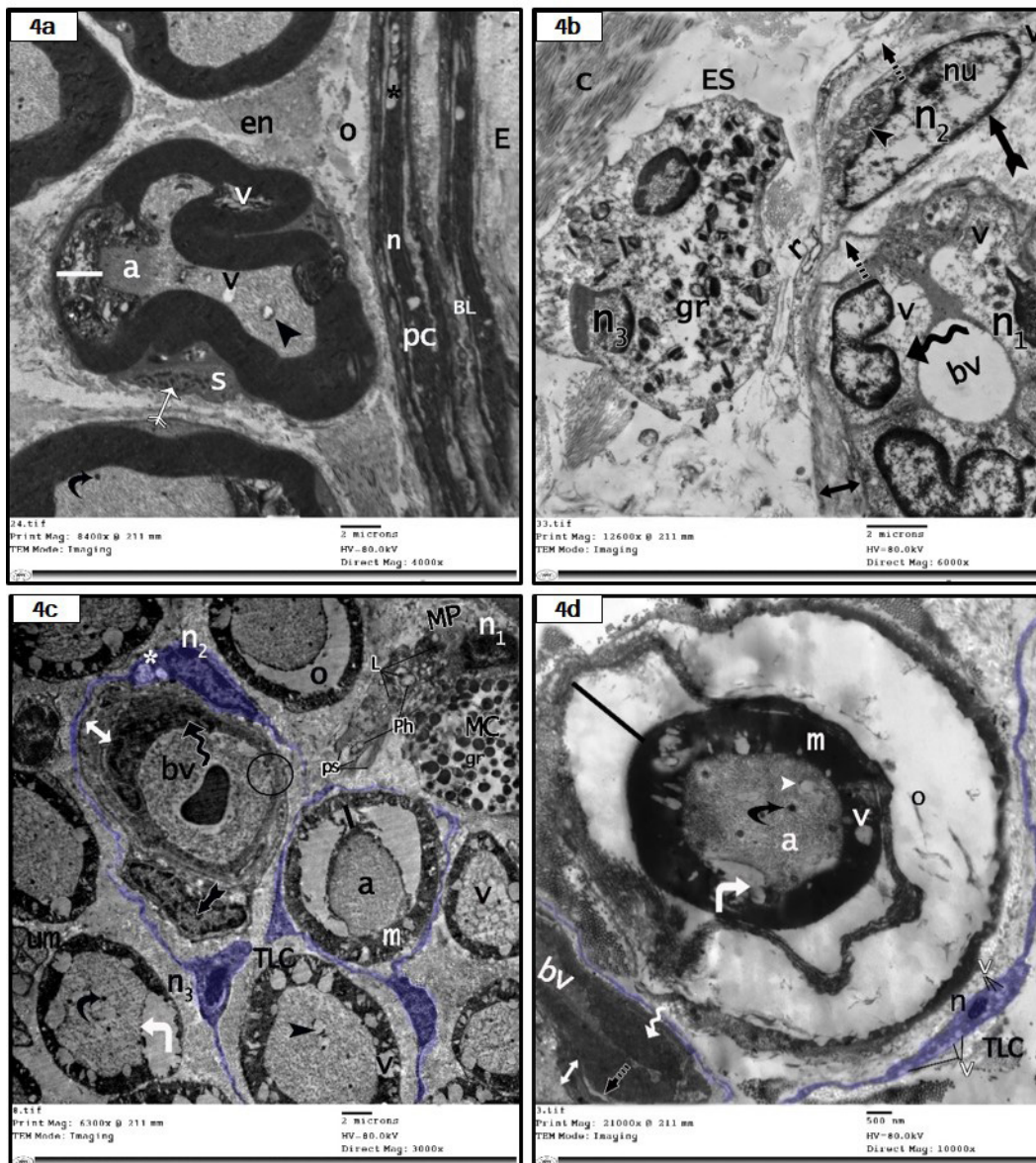


Fig. 4: TEM photomicrographs of sciatic nerve sections from diabetic group revealing: a: Part of the perineurium formed of several flat perineurial cells (PC) with flat heterochromatic nuclei (n), multiple vesicles (*) and surrounded by basal laminae (BL). Notice the presence of wide empty space (o) under the perineurium. There are myelinated fibers, their axons (a) show vacuolations (v), degenerated mitochondria (arrow head) and electron dense particles (curved arrow). Myelin split (line) and vacuolations (v) are also observed. Dense inclusions (strike arrow) in Schwann cells (S) can be seen, as well as endoneurium (en) and epineurium (E) [x4000]. b: Endoneurial blood vessel (bv) lined with endothelium (wavy arrow) showing vacuolated cytoplasm (v) and heterochromatic irregular nucleus (n1) and surrounded by thickened (double ended arrow) detached basement membrane (dashed arrows). A pericyte (bifid arrow) with slightly irregular nucleus with dissolute chromatin (n2) and small nucleolus (nu), degenerated mitochondria (arrow head), dilated rER (r) and vacuolated cytoplasm (v) is noted detached from basement membrane (dashed arrows). Eosinophil (ES) with bilobed nucleus (n), but the connecting segment is not within the plane of section, and characteristic granules (gr) with electron dense crystalline bodies surrounded by the less electron dense matrix and collagen fibrils (C) were also seen [x6000]. c: Myelinated (m) fibers, their axons (a) appear retracted (right angled arrow) or surrounded by wide empty space (o). They also reveal vacuolations (v), degenerated mitochondria (arrow head) and electron dense particles (curved arrow). Myelin split (line) and vacuolations (v) are noticed. Unmyelinated nerve fibers (um) can be seen. Endoneurial blood vessel (bv) lined with endothelial cell (wavy arrow) with disrupted junction (circle) and surrounded by thickened basement membrane (double ended arrow) enclosing a pericyte (bifid arrow). Macrophage (MP) has intended eccentric nucleus (n1) with peripheral heterochromatin, irregular surface showing pseudopodium (ps) and vacuolated granular cytoplasm rich in lysosomes (L) and phagosomes (Ph). Mast cell (MC) with electron dense granules (gr) is seen. Notice the existence of four telocyte like cells (TLC) (digitally colored blue) having characteristic telopodes communicate with each other and form sheath around blood vessel and nerve fibers. Their nuclei appear large euchromatic (n2) or small with marked heterochromatin (n3). Vesicles (*) are also seen in their cytoplasm [x3000]. d: Myelinated nerve fiber surrounded by myelin (m) exhibiting vacuolations (v) and splitting (line) with wide empty space (o). An axon (a) showing degenerated mitochondria (arrow head), electron dense particles (curved arrow) and axon retraction (right angled arrow) Narrow (collapsed) endoneurial blood vessel (bv) lined with hypertrophied endothelial cells (wavy arrow), surrounded by thickened (double ended arrow) and detached basement membrane (dashed arrow). Telocyte like cell (TLC) (digitally colored in blue) with their characteristic telopodes form sheath around nerve fiber and blood vessel (bv), its nucleus (n) appears small heterochromatic and the cytoplasm is markedly vacuolated (v) [x10000].

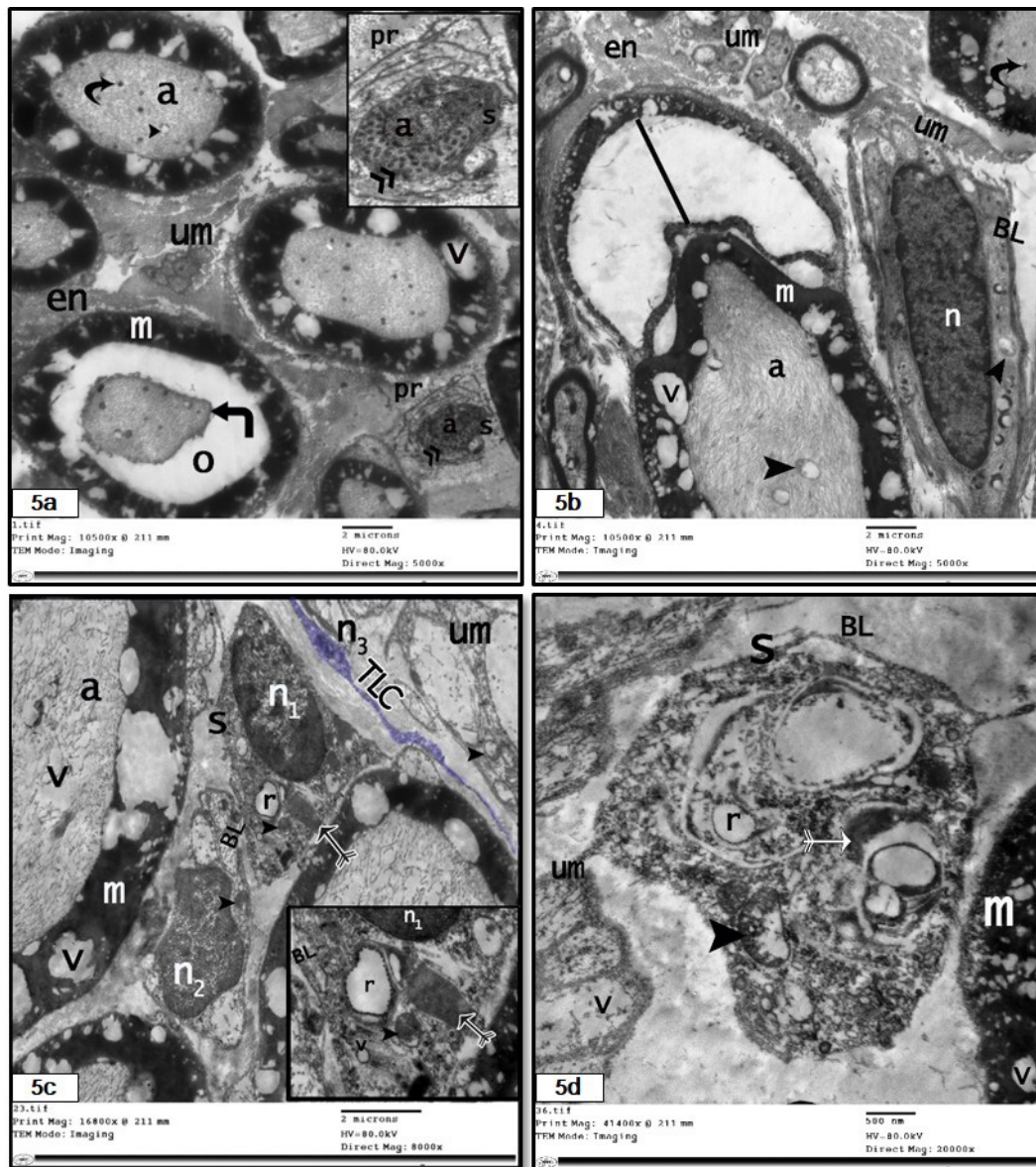


Fig. 5: TEM photomicrographs of nerve sections of diabetic group demonstrating: a: Schwann cell (S) engulfing an axon (a) surrounded by myelin debris, multiple electron dense fragments (double arrow heads) and concentrically arranged lamellae (onion bulb) formed by Schwann cell processes (pr). Myelinated nerve fibers surrounded by vacuolated (v) myelin (m), axons (a) having degenerated mitochondria (arrow head) and electron dense particles (curved arrow), retracted axon (right angled arrow) surrounded by empty wide space (o), unmyelinated nerve fibers (um) and endoneurium (en) are demonstrated [x5000, inset x15000]. b: Myelinated nerve fibers surrounded by myelin (m) showing splitting (line) and vacuolations (v). Axons (a) with degenerated mitochondria (arrow heads) and electron dense particles (curved arrow) are seen, as well, Schwann cell with oval nucleus (n) and thickened basal lamina (BL). Unmyelinated nerve fibers (um), and endoneurium (en) are noticed [x5000]. c: Myelin (m) surrounding myelinated fibers shows vacuolations (v), also axons (a) of unmyelinated fibers (um) display vacuolations (v). Two Schwann cells' nuclei (n₁ and n₂), n₂ is irregular in shape with more heterochromatin. Schwann cells (S) have thickened basal laminae (BL). Notice degenerated mitochondria (arrow heads), dilated rER (r), vacuolations (v) and large electron dense inclusion (strike arrow) in Schwann cells' cytoplasm. Telocyte like cell (TLC) (digitally colored blue) having telopodes is seen between nerve fibers, its nucleus (n₃) appears small heterochromatic [x8000, inset x20000]. d: Myelinated nerve fiber surrounded by myelin (m) revealing vacuolations (v). Unmyelinated nerve fibers (um) exhibit vacuolations (v). Schwann cell (S) has thickened basal laminae (BL), degenerated mitochondria (arrow head), dilated rER (r), vacuolations (v) and large electron dense inclusion (strike arrow) [x20000].

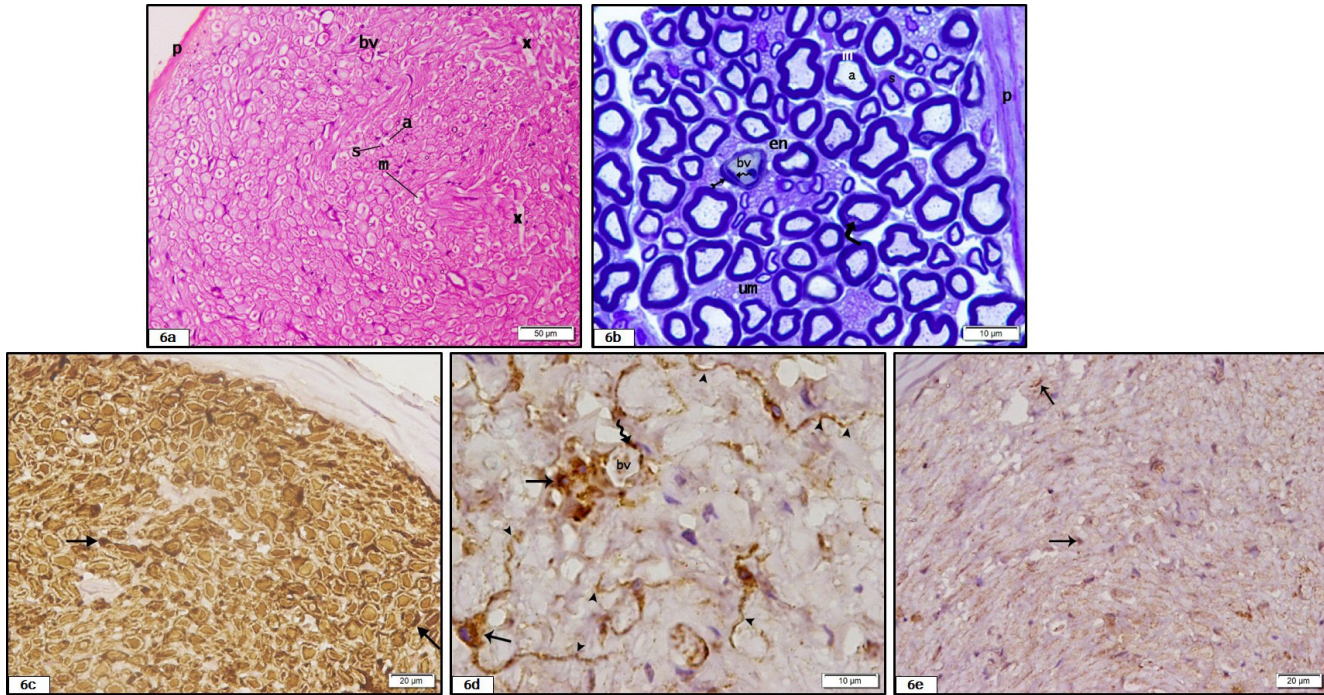


Fig. 6: Photomicrographs of sciatic nerve sections of PRP treated group showing: a: Part of apparently normal nerve bundle; axons (a), unstained myelin (m), nuclei of Schwann cells (S), endoneurial blood vessels (bv) and part of perineurium (P). Few areas of degenerated nerve fibers with empty spaces (X) are noticed [H&E, x200]. b: Numerous myelinated and unmyelinated nerve fibers (um) with variable diameters, most of them are apparently normal. Myelinated nerve fibers have axons (a) surrounded by regular myelin (m). Schwann cells (S) are seen enclosing nerve fibers. Few fibers show retracted shrunken axons (right angle arrow). Apparently normal endoneurial blood vessel (bv) with flat endothelium (wavy arrow) and pericyte (bifid arrow) is seen in endoneurium (en). Part of perineurium (P) is also observed [Toluidine blue, x1000]. c: Profuse S100+ve immunoreaction is noticed around the axons (arrows) [anti S100 immunohistochemical stain, x400]. d: Numerous CD34+ve branched cells (arrows) with brown cytoplasmic reaction and rounded nuclei are seen close to blood vessel (bv). Many CD34+ve TLCs (arrows) with their distinguishing telopodes (arrow heads) are seen around nerve fibers. Also, CD34+ve reaction is detected in endothelial cells (wavy arrow) [anti CD34 immunohistochemical stain, x1000]. e: Scanty caspase-3 immunoreaction (arrows) is seen in the endoneurium [anti caspase-3 immunohistochemical stain, x 400].

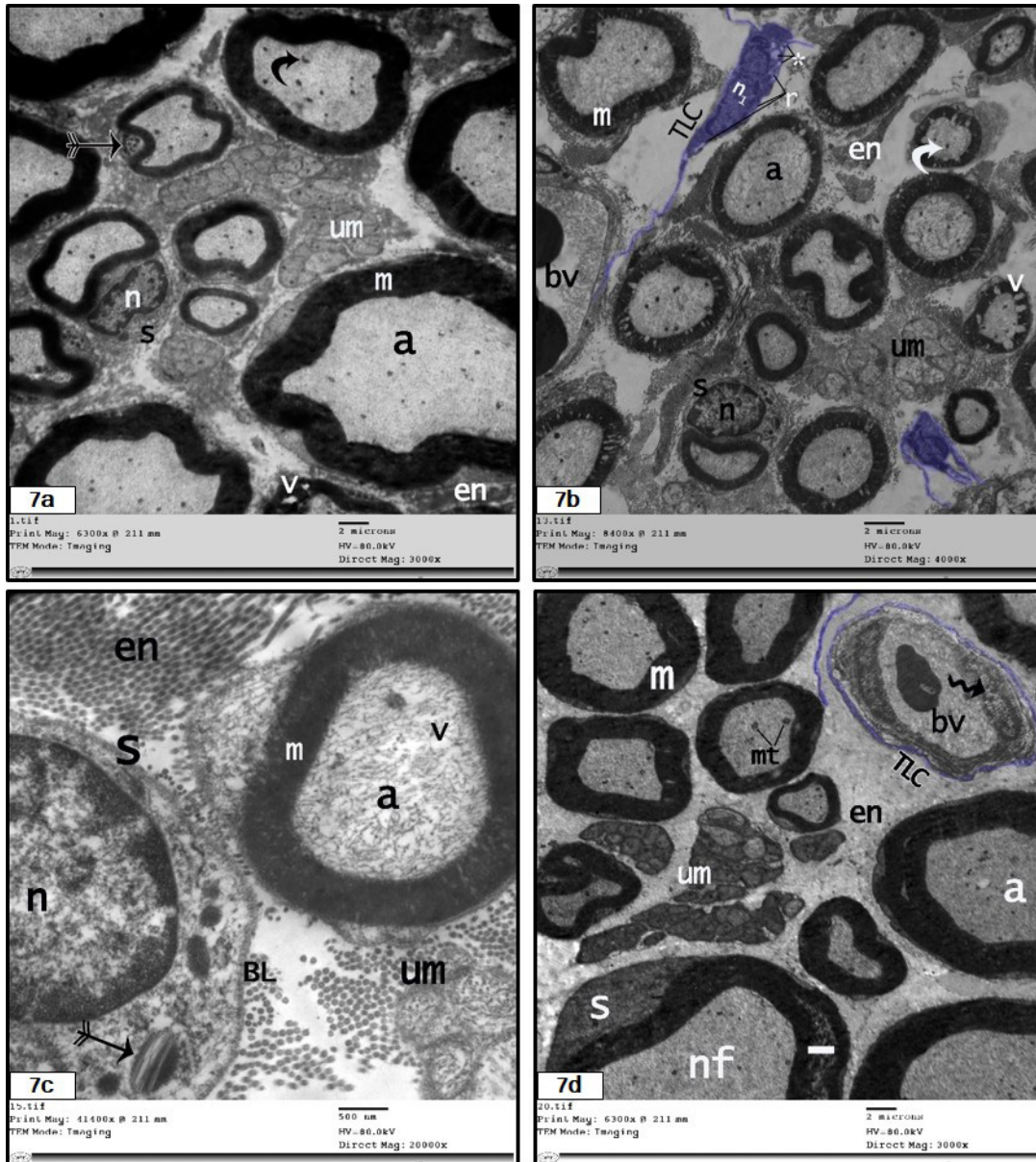


Fig. 7: TEM photomicrographs of sciatic nerve sections of PRP treated group illustrating: a: Apparently normal myelinated, unmyelinated (um) nerve fibers and endoneurium (en). Myelinated axons (a) are surrounded by regular myelin (m) and Schwann cell (S) with euchromatic nucleus. Small areas of myelin vacuolations (v), electron dense particles (curved arrow) and dense inclusions (strike arrow) in Schwann cell cytoplasm are seen [x3000]. b: Apparently normal myelinated and unmyelinated (um) nerve fibers separated by endoneurium (en). Myelin (m) reveals small areas of vacuolations (v) and axons (a) have electron dense particles (curved arrow). Schwann cell (S) and its nucleus (n) are apparently normal. Telocyte like cells (TLC) (digitally colored blue) with the distinctive telopodes, euchromatic oval nucleus (n1), rER (r) and multiple vesicles (*) are seen between nerve fibers and close to endoneurial blood vessel (bv) [x4000]. c: Higher magnification of the previous figure, showing electron dense myelin sheath (m), unmyelinated fibers (um), the axoplasm (a) contains small vacuoles (v). A Schwann cell (S) with large euchromatic nucleus (n), regular continuous basal lamina (BL) and electron dense inclusions (strike arrow) and endoneurium (en) are also noted [x20000]. d: Apparently normal unmyelinated (um) and myelinated nerve fibers (m) with endoneurium (en) in between. Axons (a) are filled with neurotubules (mt) and neurofilaments (nf) and surrounded by Schwann cells (S). Small areas of myelin split (line) are observed. Apparently normal endoneurial blood vessel (bv) lined by endothelium (wavy arrow) is seen with processes of telocyte like cells (TLC) (digitally colored blue) around it [x3000].

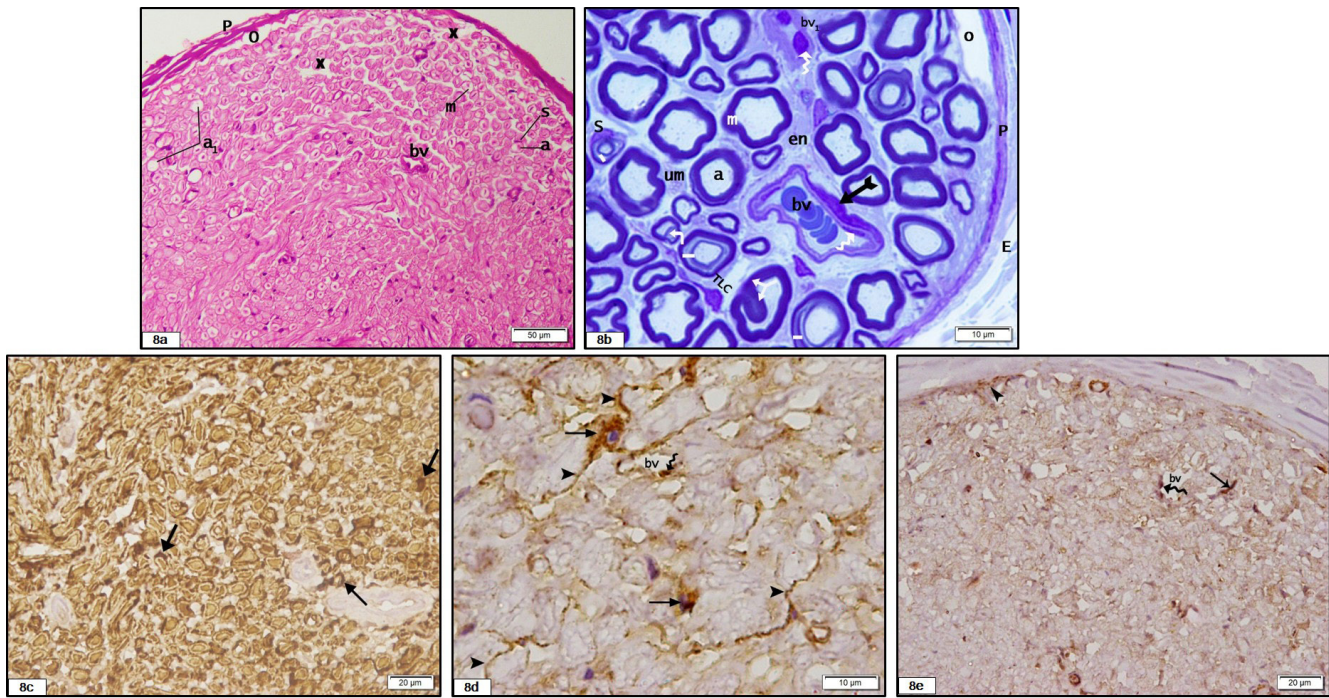


Fig. 8: Photomicrographs of sciatic nerve sections of PPP treated group revealing: a: Part of nerve bundle covered by perineurium (P) with a bit wide underlying empty space (o) and slightly less packed nerve fibers. Areas of degenerated nerve fibers and empty spaces (X). Axons (a), degenerated axons (a1), unstained myelin (m), nuclei of Schwann cells (S) and endoneurial blood vessels (bv) are seen [H&E, x200]. b: Nerve fibers, with variable diameters, have both myelinated and unmyelinated nerve fibers (um). Myelinated fibers are formed of apparently normal axons (a) enclosed by regular myelin (m). Schwann cells (S) are obviously seen enclosing nerve fibers. Some fibers have retracted shrunken axons (right angle arrow), split myelin (lines), or invaginated myelin (split arrow). Apparently normal endoneurial blood vessel (bv) with flat endothelium (wavy arrow) and another one (bv1) with high endothelium and partially narrowed lumen, endoneurium (en), Part of perineurium (P), underlying empty space (o), epineurium (E) and telocyte like cell (TLC) with the characteristic processes are also observed. [Toluidine blue, x1000]. c: Abundant S100+ve reaction is seen around axons (arrows) [anti S100 immunohistochemical stain, x 400]. d: Numerous CD34+ TLCs (arrows) with their telopodes (arrow heads) are seen around nerve fibers. CD34+ve reaction is also noted in endothelial lining (wavy arrow) of blood vessel (bv) [anti CD34 immunohistochemical stain, x1000]. e: Little caspase-3 +ve reaction is present underneath the perineurium (arrow heads), within the endoneurium (arrows) and in the endothelial cells (wavy arrow) lining the blood vessels (bv) [anti caspase-3 immunohistochemical stain, x400].

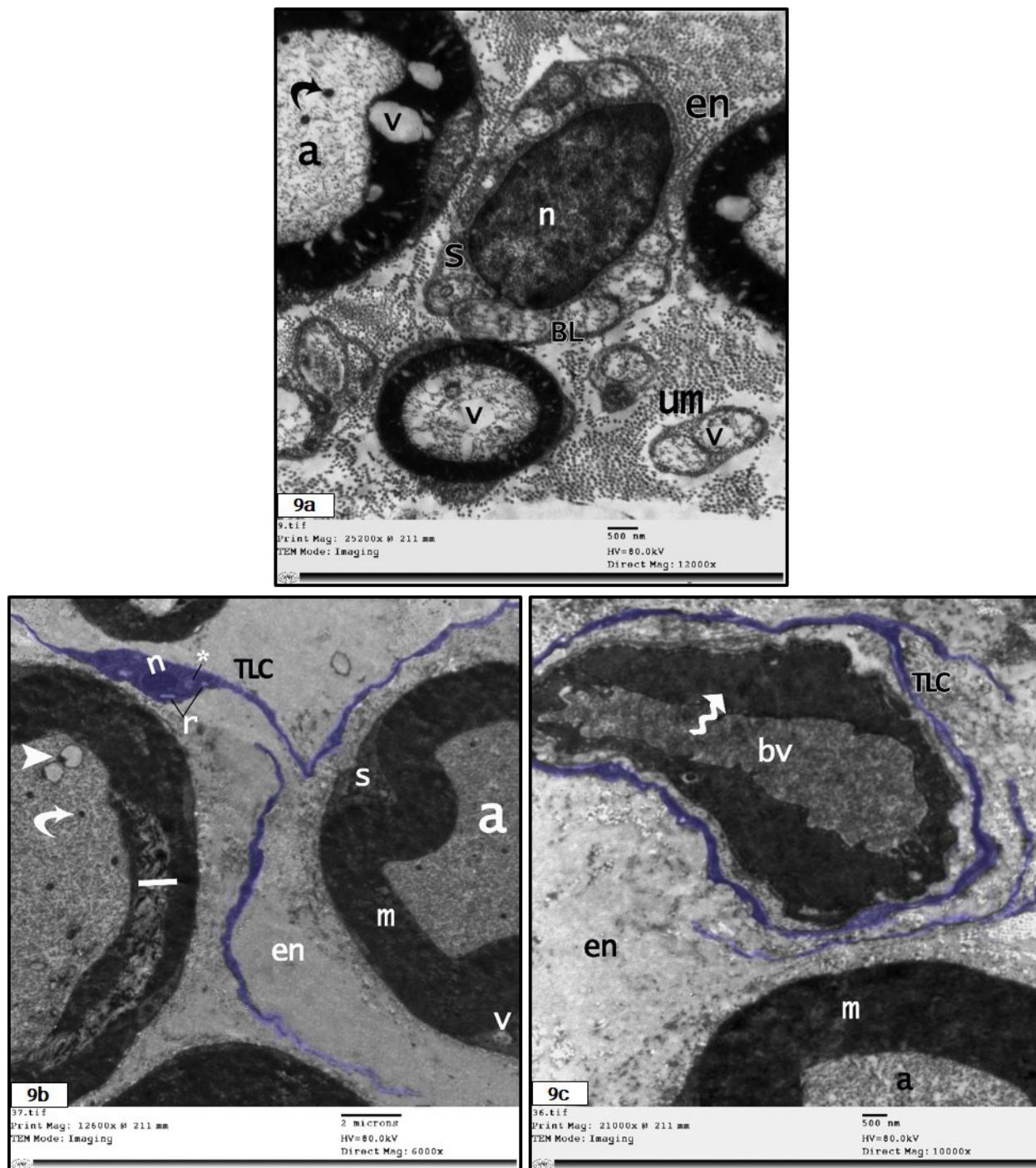


Fig. 9: TEM photomicrographs of sciatic nerve sections of PPP treated group showing: a: Myelinated and unmyelinated (um) nerve fibers separated by endoneurium (en). Regular myelin (m) reveals areas of myelin vacuolations (v), electron dense particles (curved arrow) and axonal (a) vacuoles (v) are also seen. Schwann cell (S) has apparently normal nucleus (n) and regular basal lamina (BL) [x12000]. b: Myelinated nerve fibers separated by endoneurium (en). Myelin (m) appears normal with split area (line). Axons (a) have electron dense particles (curved arrow) and degenerated mitochondria (arrow head). Small vacuole (v) is seen in Schwann cell (S). Telocyte like cell (TLC) with the characteristic telopodes (digitally colored blue), small heterochromatic oval nucleus (n), rER (r) and vesicle (*) are seen between nerve fibers [x6000]. c: Myelinated nerve fiber with normal axon (a) and myelin (m). Processes of telocyte like cells (TLC) (digitally colored blue) are seen in endoneurium (en) around an apparently normal endoneurial blood vessel (bv) lined by endothelium (wavy arrow) with slightly narrowed lumen [x10000].

Table 1: The mean values of body weight, blood glucose and NCV (\pm SD) of rats in the studied groups

Group	Mean body weight in grams \pm SD		
	Basal	Day 60	End of exp.
Group I	192.0 \pm 18.4	265.1 \pm 10.2	287.1 \pm 12.2
Group II	190.4 \pm 14.1	175.3 \pm 7.5*	167.2 \pm 7.5*
Group III	187.5 \pm 10.5	172.0 \pm 9.2*	198.0 \pm 1.2*
Group IV	185.6 \pm 10.2	170.0 \pm 7.1*	192.0 \pm 5.1*
Mean value of blood glucose (mg/dl) \pm SD			
	Basal	72 h after STZ	End of exp.
Group I	76.4 \pm 7.2	77.7 \pm 6.1	77.2 \pm 4.1
Group II	77.4 \pm 6.2	359.2 \pm 6.5*	341.3 \pm 10.3*
Group III	74.7 \pm 7.4	354.4 \pm 10.5*	299.4 \pm 9.4*
Group IV	76.8 \pm 7.4	362.2 \pm 11.5*	291.0 \pm 2.1*
Mean value of NCV (m/sec) \pm SD			
		Day 60	End of exp.
Group I		72 \pm 2	71 \pm 4
Group II		30 \pm 1*	25 \pm 2*
Group III		32 \pm 6*	64 \pm 7&
Group IV		29 \pm 4*	61 \pm 8&

* Sig as compared to group I ($p < 0.05$).&Sig as compared to group II ($p < 0.05$).**Table 2:** The mean values \pm SD of biochemical and morphometric parameters of rats in the studied groups

Parameter	Group I	Group II	Group III	Group IV
miR-146a	Day 60	1.12 \pm 0.01	0.59 \pm 0.04*	0.59 \pm 0.06*
	End of exp.	1.09 \pm 0.56	0.36 \pm 0.02*	0.96 \pm 0.02&
MDA (pg/mg)	10.63 \pm 0.01	42.72 \pm 0.51*	11.45 \pm 0.93&	13.78 \pm 3.31&
TNF α (pg/mg)	46.21 \pm 13.0	144.92 \pm 22.9*	48.56 \pm 11.6&	49.43 \pm 13.5&
NGF (ng/ mg)	64.21 \pm 8.1	18.72 \pm 0.3*	60.11 \pm 3.1&	59.41 \pm 3.5&
ZO-1	0.95 \pm 0.03	0.51 \pm 0.02*	0.77 \pm 0.05&	0.74 \pm 0.06&
Claudin-1	3.29 \pm 0.05	0.9 \pm 1.02*	2.98 \pm 0.23&	2.57 \pm 0.11&
G-ratio	0.62 \pm 0.24	0.31 \pm 0.14*	0.54 \pm 0.63&	0.51 \pm 0.42&
Capillary luminal area (μm^2)	102.1 \pm 15.3	75.1 \pm 11.2*	97.3 \pm 23.6&	95.1 \pm 13.3&
Area % of S100	3.57 \pm 0.26	1.1 \pm 0.13*	3.1 \pm 0.11&	2.8 \pm 0.32&
Number of CD34+ve	Cells in interstitium	17.3 \pm 1.89	8.6 \pm 1.17*	15.6 \pm 2.17&
	Endothelial cells	46.7 \pm 1.89	29 \pm 1.17*	39.3 \pm 1.32&
Area % of caspase-3	undetectable	1.08 \pm 0.13	0.56 \pm 0.07&	0.62 \pm 0.06&

* Sig as compared to group I ($p < 0.05$).&Sig as compared to group II ($p < 0.05$).

DISCUSSION

This is the first histological study that proved the ameliorating effect of both PRP and PPP on induced DN in albino rat and is the first to report that PPP could be to a lesser extent as beneficial as PRP in this matter; regarding the attenuation of the biochemical and histopathological alterations that occurred in the sciatic nerve.

Experimentally induced DM using STZ is a well accepted animal model to explore the behavioral, structural and pathological changes associated with DN^[23]. In the current work, a period of 60 days was chosen to establish DN as documented previously^[16]. Also its development was confirmed by the significantly reduced serum miR-146a and NCV, which is in agreement with previous studies^[14,30]. Circulating miRNAs are currently considered predictive biomarkers for diverse conditions including DM and its complications; changes in specific miRNAs levels can lead to chronic inflammation, β -cell loss/dysfunction with subsequent altered insulin secretion and signaling and diabetic complications. Recently, scientists highlight the correlation between exact miRNAs and DN onset and development^[15]; it was proved that 6 weeks of DM resulted in reduced miR-146a expression in rats's sciatic nerves, which was accompanied by significant reduction of NCV, sciatic nerve tissue damage and release of TNF- α ^[14]. Besides, diabetic rats recorded significant weight loss compared to control and this is in accordance with former studies^[22, 23, 31]. Reduction in the body weight could be due to hyperglycemia resulting in glucosuria and dehydration, also might be due to hypoinsulinemia resulting in loss of tissue proteins and muscle wasting or adipose tissue loss to produce energy^[23].

Additionally, the present study established an association between DN development and elevated levels of oxidative (MDA) and proinflammatory (TNF- α) cytokines detected in the sciatic nerves of diabetic rats which goes in line with earlier studies^[22, 23, 32]. It has been suggested that oxidative stress (OS) is an imperative pathological mechanism underlying DN and is involved in the development of other DM complications, diminished endoneurial blood flow and sciatic nerve dysfunction were observed in diabetic rats exposed to OS with increased oxidative enzymes in the nerve tissue^[22]. Neuronal OS can also activate multiple kinases that have fundamental role in triggering a cascade of chemokines and cytokines production as proinflammatory interleukin-1 α (IL-1 α), 1 β , -2, -6, and -8, and TNF α , which enhance the existing immune and inflammatory responses that further augment the cellular OS, endorsing more neuronal damage and peripheral nerve injury in experimental models of DN^[23,33].

Nerve growth factor (NGF), an integral neuronal protein; implicated in nerve cell development, and maintenance; it has a neuroprotective function with the capacity to potentiate axonal growth, and pathological disorders altering its level result in loss of neurons' function and their death^[16]. The present work reported significantly reduced NGF in the sciatic nerves of DN group, indicating an increased nerve

cell apoptosis with consequent decreased nerve integrity and this is in agreement with previous studies^[22, 23, 34]. Low NGF level in DN might be due to either its decreased production or transport, possibly because of the OS resulting from hyperglycemia, also autoimmunity may contribute to its deficiency by neutralization of the existing NGF; there are biochemical and structural similarities between it and insulin, so antibodies to insulin might cross-react with NGF reducing its accessibility to nerves, accordingly contributing to DN development^[23].

Histologically, neuropathy was evident in sciatic nerve sections from DN group and this is consistent with former studies^[31,32]. There was marked axonopathy with abnormal myelin figures and this was established by the significantly reduced G-ratio (an important indicator for myelinated fiber function^[27]), which could be attributed to either reduced axon diameter (retracted, shrunken or degenerated) or increased fiber diameter caused mostly by myelin splitting or its irregular thickening due to the injury of myelin producing SCs; Schwannopathy.

Most researches have concentrated on diabetic axonopathy; but nowadays there is better understanding of the molecular changes in SCs that highlights the impact of Schwannopathy in the occurrence and advancement of DN. Schwann cells ensheathe all axons either myelinated or not and they are active partners not just passive insulators that are capable of altering nerve cell biology through metabolic support and adjusting responses to tissue injury. Disturbed SCs function compromises axon-glial interaction and nerve homeostasis, resulting in neurodegeneration and damage of nerve fiber. When pathology develops, slight segmental demyelination followed by remyelination starts with the existence of normal axons; indicating that Schwannopathy constitutes the first step in DN pathogenesis^[35].

In the present study, SCs revealed thickened basal laminae, irregular heterochromatic nuclei, degenerated mitochondria, dilated rER, vacuolated cytoplasm; that could be attributed to the numerous diabetic stressors that increase SCs dysfunction and apoptosis and this was confirmed by the significant decreased S100 and increased caspase-3 immunoreaction in DN group. When SCs were cultured previously in hyperglycemic environment, they changed their morphology; appearing with small cell bodies and their processes failed to grow, with increased apoptotic events as caspase-3 cleavage and DNA fragmentation^[36]. In addition, mitochondrial dysfunction has been linked to DN pathogenesis in several ways; hyperglycemia results in altering of mitochondrial proteome within SCs, also results in deficient respiratory competence in SCs, initiated by increased oxygen consumption, leading to defective oxidative phosphorylation^[37]. Moreover, mitochondrial dysfunction is accompanied by disturbed calcium homeostasis and acylcarnitines accumulation that upon release induce axonal degeneration^[35].

Furthermore, SCs were found to dedifferentiate and accustom a repair-mediating phenotype necessary for myelin

degradation as well as nerve regeneration when exposed to deleterious factors possibly OS and inflammation^[38]. Nerves remove myelin by two different mechanisms; 1st, SCs change from myelin preservation to fragmentation through its autophagy and delivering it to SCs as myelin ovoids and forms smaller cytoplasmic myelin fragments followed by lysosomal degradation, 2nd, macrophages recruited by cytokines invade injured nerves and phagocytose myelin debris^[39]. The previous data could explain the large dense inclusions and myelin figures detected in SCs in the current work and this is in harmony with former studies^[40].

On the other hand, with constant exposure to injurious factors as hyperglycemia, enhanced immune responses are created where SCs have been accepted as immune-competent cells; producing numerous cytokines and inflammatory mediators involved in the pathogenesis of DN and play a role in the recruitment of different immune cells such as eosinophils, mast cells and macrophages, which sequentially triggers apoptosis, inducing SCs damage^[38].

In this work, the recruitment of immune cells and macrophages was obvious in sciatic nerve sections from DN group and this is an important event in the pathogenesis of nerve injury; as macrophages are crucial in tissue injury and repair via cytokines secretion^[41]. This could be elucidated by the release of monocyte chemoattractant protein-1, IL-1 α and -1 β released from affected nerves^[42]. In nerve injuries, inflammation leads to local hypoxia and necrosis and these are the main obstacles for nerve regeneration and repair, which needs a good microenvironment, clean of necrotic fragments to promote angiogenesis and SCs proliferation and migration^[43]. Macrophages, including differentiated SCs, have two actions; pro-inflammatory (M1) and anti-inflammatory (M2), and their co-action generates good microenvironment for tissue repair. M1 and M2 macrophages sustain a condition of active equilibrium and exchanging of phenotype along with function which is synchronized by modifying signals^[41]. In addition, they were proved to activate the proliferation and division of SCs precursors, which have stronger phagocytic and secretory capacity aiding in debris removal and increasing the release of NGF and brain-derived growth factor^[44]. Furthermore, macrophages can sense and respond to hypoxia by activating hypoxia inducible factor 1 α that stimulates angiogenesis via VEGF^[43].

Sciatic nerve sections from DN group displayed features of microangiopathy that is consistent with earlier studies^[16,28]; there were obvious alterations in both the ECs and pericytes, with their underlying thickened and/or interrupted basement membranes and disrupted junctions. Some vessels with narrow lumens were also noted which could be attributed to the high ECs. This was verified by the significantly decreased capillary luminal area, ZO-1 and claudin-1, in addition to the significant decrease in CD34 and increase in caspase-3 immunoexpression in ECs compared to the control group. The vascular integrity of endoneurial capillaries is a significant determinant for nerve degeneration way more than the endoneurial capillary density^[28], which in turn impacts NCV; it was reported that sciatic nerves in DN

models exhibited decreased endoneurial oxygen tension due to decreased blood flow, which was accompanied by reduced NCV in the same proportion^[5]. DN is believed to result from two chief mechanisms; hyperglycemia-induced damage to nerve cells and nerve ischemia from reduced neurovascular flow^[16]. The vascular alterations in this work highlight the compromise in the function of BNB which consists of ECs, pericytes and basement membranes.

A crucial component of BNB in both the perineurium and ECs is the TJs. Endothelial cells in BNB express ZO-1 and -2 and claudins (1, 2, 5, and 19), whereas perineurial cells express claudin-1^[2,12]. Endothelial dysfunction results from inhibition of some glycolytic enzymes with accumulation of several intermediates triggering diverse inflammatory pathways, which produce numerous metabolites (as protein kinase C, hexosamines and polyols) capable of damaging the nerve. Also it results from the imbalance between reactive oxygen species formation and mitochondrial redox state^[5,45]. Regarding the pericytes, they strengthen the BNB by increasing claudin-5 expression and by acting as paracrine cells; they express a number of GFs, as VEGF, important for BNB maintenance and regulation. In DM, pericytes are frequently lost, so their paracrine role is missing or extensively diminished, resulting in breakdown of BNB. Additionally, the diabetic environment was found to increase collagen type IV and fibronectin production by pericytes and these are key constituents in BNB basement membrane^[46], which could explain the thick basement membrane seen in the endoneurial capillaries of DN group (group II). Furthermore, it has been suggested that hypoxia opens BNB via VEGF pathway (upregulated in macrophages) and alters the permeability of microvessels. Besides, there is increased endoneurial concentration of large molecules like IgM, IgG and mannitol and albumin, leading to disturbed osmotic balance and increased BNB permeability^[2], which could explain the detected edema in sciatic nerve sections from DN group.

In the present study, the perineurial cells displayed heterochromatic nuclei, confirmed by positive caspase-3 immunoreaction and decreased claudin-1 expression, this resulted in TJs disruption that in turn provides another explanation for the underlying edema. Due to the vital role of perineurium in maintaining the homeostasis of endoneurial microenvironment; it is obvious that apoptosis of its cells with disruption in their TJs could be an imperative factor in DN. Numerous studies have reported the implication of perineurium and TJs in different neuronal pathologies like multiple sclerosis, autonomic peripheral neuropathies, ischemic stroke and Alzheimer's disease. Moreover, breakdown of TJs helps inflammatory cytokines to enter into the endoneurium worsening the neuropathy^[10,12].

Telocyte like cells (TLCs), in addition to BNB and perineurial cells, reinforce the nerves' protecting barrier; as they form sheath around blood vessels and nerve fibers and beneath the perineurium^[13]. In the current work, they were manifested by TEM, their slender telopodes and absent basement membranes, and the positive CD34

immunoreaction beneath the perineurium and in the endoneurium. Telocytes disturbance in number or loss of relations was associated with many diseases, and the present work proved their involvement in the pathological process of DN; many appeared with apoptotic nuclei, however, some appeared normal with euchromatic nuclei as if trying to limit the disease. Also sciatic nerve sections from DN group revealed much less TLCs than the control and this was confirmed by the significant reduction in CD34 and increased caspase-3 immunoreactivity in the interstitium.

Plasma fractions; PRP and PPP have platelets counts correspondingly higher and lower than their standard levels in blood^[9]. Platelet rich plasma has been used in earlier studies and proved its beneficial effects in different fields; skeletal muscle repair and regeneration^[47], autologous nerve grafts^[48], spinal cord injury^[49] and peripheral nerve injury^[6]. In addition, allogenic PRP application has yielded safe and encouraging results in treating musculoskeletal conditions; so opens novel viewpoints regarding off-the-shelf PRP treatment to patients who cannot receive autologous PRP^[9]. Moreover, it has been evidenced that the benefits of PRP are mostly due to plasma by itself; so PPP, despite having much less platelets, still represents a reservoir of bioactive molecules and GFs^[50].

In the present work both groups III and IV showed decrease in blood glucose level compared to DN group and this goes in line with other scientists^[17] who explained it by neo-vascularization and restoration of pancreatic islet cell mass after PRP treatment. This decreased glucose level might explain the significant increase in the body weights in these groups. In addition, there was significant reduction in the oxidative marker MDA in both groups III and IV which is consistent with former studies^[22,51]. This could be clarified by the ability of PRP to activate phosphatidylinositol-3 kinase pathway that can reduce reactive oxygen species production and increase the resistance to oxidation^[52]. Adding up, there was significant reduction in the proinflammatory marker TNF α after plasma treatment, which is consistent with Tong *et al.*^[53] who stated that PRP reduced both cellular and humoral immune responses that had beneficial effects on histological parameters. This could be attributed to PRP high content of hepatocyte growth factor that was proved to have an anti-inflammatory effect in different organs as kidney, lung and liver^[54]. Also, PRP contains a considerable amount of chemokine ligand-5 that inhibits numerous cytokines released by immune cells and elevates the concentration of anti-inflammatory lipoxin A4, leading to resolution of inflammation^[55].

Histological examination of sciatic nerve sections from plasma treated groups displayed picture almost comparable to the control; this is due to its supra-physiological concentrations of GFs that play essential roles in neovascularization, wound healing and tissue regeneration^[56]. Beside GFs, platelets stimulation makes them secrete extracellular vesicles, including exosomes, which act as carriers for messenger RNAs and microRNAs that have vital role in platelet-cell and cell-cell communications^[57].

The current study revealed recovery of nerve fibers regarding the axons and their myelin sheathes with almost normal appearance of SCs, confirmed by the significant increase G-ratio, NCV and S100 immunoreaction, and this is in harmony with previous studies^[7,48]. This could be attributable to plasma content of VEGF, epithelial growth factor, insulin like growth factor-1 (IGF-1), platelet-derived growth factor (PDGF) in addition to transforming growth factor- β 1 (TGF- β 1); which are linked to nerve fibers repair and remyelination^[7,50]. It was found that neurons and SCs express receptors for PDGF that functions as survival factor and mitogen for SCs and neurons, TGF β 1 as well is essential for proliferation and differentiation of SCs and is important for the neurotrophic effects of several other GFs^[58]. Moreover, PRP speeds up nerve regeneration indirectly by activating SCs to produce neurotrophic factors as glial derived neurotrophic factor and NGF^[7]. Sciatic nerve preservation could elucidate the significant elevation in NGF expression and serum miR-146a found in both groups III and IV compared to group II.

Herein, there was preservation of vasculature; capillaries luminal areas, ECs and pericytes that was confirmed by the significant increase in CD34 positive ECs. Former studies have proved the angiogenesis effect of PRP in different tissues; lung injury^[59] and traumatic skeletal muscle injury where a significant increase in CD34 immunopositive ECs lining newly formed capillaries after PRP treatment was found^[60]. Blood vessels do not only convey oxygen and nutrients; they also provide informative signals to the surrounding microenvironment, thus, angiogenesis is fundamental in tissue regeneration and its targeting is good policy to regenerate damaged or lost tissues^[59]. Most existing therapies rely on using single factor as VEGF, though, angiogenesis is controlled by several signaling pathways and a proper mixture of these factors is preferred to get stable functional vessels in the tissue^[61].

Platelets store and release many angiogenesis factors (PDGF, angiopoietin-1, TGF- β , basic fibroblast growth factor (bFGF) and VEGF) and attract ECs, stem cells and macrophages to injured sites, thus enhance angiogenesis and tissue regeneration^[62]. Nevertheless, the signaling mechanisms by which PRP controls angiogenesis are still under research; an earlier study stated that many of the angiogenesis effects of VEGF are mediated by VEGF receptor-2, where their binding activates receptor kinase activity and attract signaling enzymes necessary for ECs survival, proliferation, migration and tube formation. This study also proposed that VEGF and bFGF could be encapsulated into exosomes and carried to affected tissues to promote angiogenesis in ECs^[63]. Another explanation was provided by Mammoto *et al.*^[59] who have reported that PRP contains abundant angiopoietin-1 that maintains vascular integrity and stimulates new vessels formation via the activation of angiogenesis receptor tyrosine-protein kinase (Tie2) in ECs speeding up their sprouting. Moreover, platelets directly promote neovascularization and their alpha granules are chief source of PDGF known to contribute in angiogenesis, matrix synthesis and wound healing^[64].

Furthermore, examined sections from plasma treated groups showed significant decrease in caspase-3 immunoreactivity, which goes in line with previous studies that have proved the antiapoptotic effect of PRP on chondrocytes^[65] and renal cells^[19,51], and this cellular preservation might explain the subsequent preservation of TJs and the significant elevation in ZO-1 and claudin-1 expression in this study. This antiapoptotic effect was previously explained by decreased mRNA level of Bcl-2-associated death promoter and increase in the mRNA level of antiapoptotic Bcl-2^[8,65]. Also TGF-β1, in plasma, directly increases Bcl-2 expression and maintains cellular homeostasis which guard against apoptosis, besides, the improvement in tissue vascularity by VEGF shares in protecting against apoptosis^[19]. Moreover the antiapoptotic outcome could be attributed to the antioxidant and anti-inflammatory effects of PRP^[51, 54].

An outstanding finding in these two groups is the evident increase in TLCs number when compared to the DN group; as was established by significantly increased CD34 positive cells in the interstitium. Increasing evidence has pointed toward TCs as being located in stem cell niches forming a complex network with blood vessels, resident stem cells, nerve endings and other interstitial components, thus prominently contribute to tissue repair and regeneration^[66] and these stem cells were noticeable in CD34 immunostained sections. In addition, previous studies have proved the efficacy of PRP in the repair and regeneration of muscle fibers, this was achieved by stimulation of bone marrow derived stromal cells, survival and differentiation, including TCs^[9, 47]. TCs presence in plasma treated groups in this work might point to their role in peripheral nerve repair and regeneration; as they make contacts with ECs, pericytes, SCs, plus other interstitial cells, macrophages and mast cells^[66]. This goes in harmony with several studies that discussed the regenerative potential of TCs in different tissues; Marini *et al.*^[67] proved their role in skeletal muscle regeneration which has occurred via their telopodes connecting with each other and with satellite cells, develop three-dimensional network that functions as a scaffold carrying signals for lengthy distances and guides the migration and proliferation of satellite cells, plus paracrine modulation of their function via the release of extracellular vesicles that contain miRNAs or myogenic factors like VEGF. Besides it has been reported that TCs three-dimensional network supports cardiac progenitor cells reflecting their impending role in the repair of damaged myocardium^[68]. Furthermore, it was found that paracrine signaling mediated via miRNAs between TCs and stem cells occurs in different tissues; as several miRNAs with proangiopoietic potential are expressed by TCs as miR-126, 130 and 24. Also, shed vesicles and exosomes containing various miRNAs were identified along the telopodes or releasing from them in different tissues undergoing repair or regeneration as lung, cardiac and skeletal muscles^[66], and these vesicles were noticed in the cytoplasm of TLCs in sections from group III.

The findings of the PRP group could be contradictory to numerous studies^[6, 49], even so, might be explained by more than one way; some scientists reported that cells viability and proliferation could be suppressed by PRP in higher concentrations, which suggests a dose-dependent PRP preparations^[69]. Also an earlier study reported that the most copious platelets miRNA; miR-223, could induce ECs apoptosis and reduce the level of IGF-1 receptor^[70]. In addition, it was found that PRP contains a greater quantity of GFs unfavorable for myoblast differentiation as TGFβ-1^[71]. Hence, PPP may hold promise for their reparative and regenerative potentials, especially when compared to PRP regarding its cost^[72]. As well, miRNAs in PRP are affected by cycles of freezing and thawing and by incubation for 24 h at room temperature, in contrast, these have no evident effect on the abundance of miRNA in PPP; as platelets that contain the bulk of miRNAs in PRP are more vulnerable to these two factors than small carriers of miRNA as extracellular vesicles or plasma miRNAs that are left behind after platelets removal^[73].

Platelet poor plasma, widely considered waste product of PRP, has been recently recognized to exert a favorable effect on several tissues^[9]. Although it contains a low platelets concentration and consequently lesser quantities of GFs, it remains a reservoir for bioactive molecules, like PDGF, TGF-β and IGF-1^[50]. In the present study, PPP proved to have comparable results to PRP, concerning the antioxidant, anti-inflammatory, regenerative and angiogenesis effects on sciatic nerve tissue. This coincides with earlier studies that confirmed the antioxidant and anti-inflammatory effects of PPP^[74] and proved its beneficial role in different tissues; in chronic diabetic foot ulcers, PPP gave the same results as PRP in healing the ulcers and reducing the associated inflammation^[75]. Also, PPP had positive outcomes on gingival repair through myofibroblast differentiation differentiation and production of structural molecules of the extracellular matrix^[76] and had a proliferative effect on bone differentiation as well^[19]. Likewise, PPP significantly induced myoblasts into muscle differentiation pathway necessary for skeletal muscle regeneration^[71]. Additionally, Shahidi *et al.*^[69] examined the angiogenesis effect of PPP in-vivo on skin wound and in-vitro on human umbilical vein ECs. They documented a significant increase in CD34 and VEGF receptor-2 expression, and unexpectedly, their levels after PRP were less than after PPP treatment and this was confirmed by increased angiogenesis in-vivo after using PPP. Yet, healing linked to angiogenesis was observed at day 10 after treatment with both PPP and PRP.

CONCLUSION

The data of the present work has proved that either PPP or PRP might be a promising ameliorative therapy in DN; *via* attenuating the biochemical and histopathological alterations in sciatic nerve. They have both reduced the hyperglycemia, oxidative and inflammatory stresses and apoptosis, as well as, improved nerve regeneration and angiogenesis and preserved TLCs.

CONFLICT OF INTERESTS

There are no conflicts of interest.

REFERENCES

1. Dewanjee S, Das S, Das AK, Bhattacharjee N, Dilhingia A, Dua TK, Kalita J, Manna P. Molecular mechanism of diabetic neuropathy and its pharmacotherapeutic targets. *Eur J Pharmacol.* 2018; 15: 833:472-523.
2. Richner M, Ferreira N, Dudele A, Jensen TS, Vaegter CB, Gonçalves NP. Functional and structural changes of the blood-nerve-barrier in diabetic neuropathy. *Front Neurosci.* 2019; 12:1038.
3. Hinder LM, Murdock BJ, Park M, Bender DE, O'Brien PD, Rumora AE, Hur J, Feldman EL. Transcriptional networks of progressive diabetic peripheral neuropathy in the db/db mouse model of type 2 diabetes: an inflammatory story. *Exp Neurol.* 2018; 305: 33–43.
4. Tesfaye S, Selvarajah D. Advances in the epidemiology, pathogenesis and management of diabetic peripheral neuropathy. *Diabetes Metab Res Rev.* 2012; 28: 8–14.
5. Kobayashi M, Zochodne DW. Diabetic neuropathy and the sensory neuron: New aspects of pathogenesis and their treatment implications. *J Diabetes Investig.* 2018; 9: 1239–54.
6. Bastami F, Vares P, Khojasteh A. Healing effects of platelet-rich plasma on peripheral nerve injuries. *J Craniofac Surg.* 2017; 28: e49-e57.
7. Salarinia R, Sadeghnia HR, Alamdari DH, Hoseini SJ, Mafinezhad A, Hosseini M. Platelet rich plasma: effective treatment for repairing of spinal cord injury in rat. *Acta Orthop Traumatol Turc.* 2017; 51:254–7.
8. Salem N, Helmi N, Assaf N. Renoprotective effect of platelet-rich plasma on cisplatin-induced nephrotoxicity in rats. *Oxid Med Cell Longev.* 2018; 2018: 9658230.
9. Chellini F, Tani A, Zecchi-Orlandini S, Sassoli C. Influence of platelet-rich and platelet-poor plasma on endogenous mechanisms of skeletal muscle repair/regeneration. *Int J Mol Sci.* 2019; 20:683.
10. Reinhold AK, Rittner HL. Barrier function in the peripheral and central nervous system-a review. *Pflugers Arch.* 2017; 469:123–34.
11. Jesuraj NJ, Santosa KB, Macewan MR, Moore AM, Kasukurthi R, Ray WZ, Flagg ER, Hunter DA, Borschel GH, Johnson PJ, Mackinnon SE, Sakiyama-Elbert SE. Schwann cells seeded in acellular nerve grafts improve functional recovery. *Muscle Nerve.* 2014; 49:267–76.
12. Sharifi Pasandi M, Hosseini Shirazi F, Gholami MR, Salehi H, Najafzadeh N, Mazani M, Ghasemi Hamidabadi H, Niapour A. Epi/perineural and Schwann cells as well as perineural sheath integrity are affected following 2,4-d exposure. *Neurotox Res.* 2017; 32: 624–38.
13. Mirancea N. Telocyte - a particular cell phenotype. Infrastructure, relationships and putative functions. *Rom J Morphol Embryol.* 2016; 57: 7-21.
14. Feng Y, Chen L, Luo Q, Wu M, Chen Y, Shi X. Involvement of microRNA-146a in diabetic peripheral neuropathy through the regulation of inflammation. *Drug Des Devel Ther.* 2018; 12:171–7.
15. Simeoli R, Fierabracci A. Insights into the Role of MicroRNAs in the Onset and Development of Diabetic Neuropathy. *Int J Mol Sci.* 2019; 20: 4627-36.
16. Oghbaei H, Mohaddes G, Hamidian G, Keyhanmanesh R. Sodium nitrate preconditioning prevents progression of the neuropathic pain in streptozotocin-induced diabetes wistar rats. *J Diabetes Metab Disord.* 2020; <https://doi.org/10.1007/s40200-019-00481-4>.
17. El-Tahawy NF, Rifai RA, Saber EA, Saied SR, Ibrahim RA. Effect of platelet rich plasma (prp) injection on the endocrine pancreas of the experimentally induced diabetes in male albino rats: a histological and immunohistochemical study. *J Diabetes Metab.* 2017; 8: 730-9.
18. Pazzini JM, Nardi AB, Huppes RR, Gering AP, Ferreira MG, Marília GPA., Silveira Camila PB, Luzzi Mayara C, Santos Romeu. Method to obtain platelet-rich plasma from rabbits (*Oryctolagus cuniculus*). *Pesquisa Veterinária Brasileira* 2016; 36: 39-44.
19. Martín-Solé O, Rodó J, García-Aparicio L, Blanch J, Cusí V, Albert A. Effects of platelet-rich plasma (PRP) on a model of renal ischemia-reperfusion in rats. *PLoS ONE.* 2016; 11(8): e0160703.
20. Nukada, H., Baba, M., Ogasawara, S., McMorrان, D. and Yagihashi, S. Neuropathy in the spontaneously hypertensive rat: An electrophysiological and histological study. *Muscle Nerve* 2016; 54: 756-62.
21. Pourghasem M, Nasiri E, Shafi H. Early renal histological changes in alloxan-induced diabetic rats. *Int J Mol Cell Med.* 2014; 3:11–5.
22. Fatani AJ, Al-Rejaie SS, Abuhashish HM, Al-Assaf A, Parmar MY, Ola MS, Ahmed MM. Neuroprotective effects of Gymnema sylvestre on streptozotocin-induced diabetic neuropathy in rats. *Exp Ther Med.* 2015; 9: 1670-8.
23. Allam MM, Muhammad MH. Effects of moderate exercise training and detraining on diabetic peripheral neuropathy in streptozotocin-induced diabetic rats. *Benha Med J.* 2018; 35: 150-6.

24. Suvarna K, Layton C, Bancroft J. The Hematoxylin and eosin, Immunohistochemical techniques and Transmission electron microscopy In: Bancroft's Theory and practice of Histological Techniques, 7th ed. Churchill Livingstone Elsevier, Oxford. 2013; pp. 173-86, 187-214 and 493-38.
25. Liu D, Liang X, Zhang H. Effects of high glucose on cell viability and differentiation in primary cultured Schwann cells: potential role of ERK signaling pathway. *Neurochem Res*. 2016; 41: 1281-90.
26. Dykstra MJ and Reuss LE. Staining methods for semithins and ultra thins. In: Biological electron microscopy, theory, techniques and troubleshooting, 2nd ed. Kluwer Academic Publishers/Plenum Publishers. 2003; pp.175- 96.
27. Hassen E, mahmod A, Ibrahim N, El-Shal A. The Effect of Long Term Administration of Aspartame on the Sciatic nerve of adult male albino rats and the possible therapeutic role of ozone (histological and biochemical study), *Egyptian Journal of Histology* 2019; 42: 191-201.
28. Kan HW, Hsieh JH, Chien HF, Lin YH, Yeh TY, Chao CC, Hsieh ST. CD40-mediated HIF-1 α expression underlying microangiopathy in diabetic nerve pathology. *Dis Model Mech* 2018; 11: dmm033647.
29. Emsley R, Dunn G, White IR. Mediation and moderation of treatment effects in randomised controlled trials of complex interventions. *Stat Methods Med Res* 2010; 19: 237-70.
30. Shi X, Chen Y, Nadeem L, Xu G. Beneficial effect of TNF- α inhibition on diabetic peripheral neuropathy. *J Neuroinflammation* 2013; 10: 836.
31. Afifi N. Neuroprotective effect of melatonin in a rat model of streptozotocin-induced diabetic neuropathy: Light and electron microscopic study. *The Egyptian Journal of Histology* 2013, 36:321-35.
32. Elgayar SA, Eltony SA, Sayed AA, Abbas AY. Protective effect of vitamin B complex in diabetic peripheral neuropathy - Histopathological study. *Eur J Anat* 2017; 21: 173-87.
33. Feldman EL, Nave KA, Jensen TS, Bennett DLH. New Horizons in Diabetic Neuropathy: Mechanisms, Bioenergetics, and Pain. *Neuron* 2017; 93: 1296-313.
34. Chen J. Clinical observation of mouse nerve growth factor for injection for treatment of diabetic peripheral neuropathy. *Chinese Med Guide* 2013; 11:571-2.
35. Gonçalves NP, Vægter CB, Pallesen LT. Peripheral Glial Cells in the Development of Diabetic Neuropathy. *Front Neurol* 2018; 9: 268-76.
36. Liu D, Liang X, Zhang H. Effects of high glucose on cell viability and differentiation in primary cultured Schwann cells: potential role of ERK signaling pathway. *Neurochem Res* 2016; 41: 1281-90.
37. Freeman OJ, Unwin RD, Dowsey AW, Begley P, Ali S, Hollywood KA, et al. Metabolic dysfunction is restricted to the sciatic nerve in experimental diabetic neuropathy. *Diabetes* 2015; 65: 228-38.
38. Tzekova N, Heinen A, Küry P. Molecules involved in the crosstalk between immune- and peripheral nerve Schwann cells. *J Clin Immunol* 2014; 34: 86-104.
39. Jessen KR, Mirsky R. The success and failure of the Schwann cell response to nerve injury. *Front Cell Neurosci* 2019; 13:33.
40. Bahaa A, Omet A. Electron microscopic study of acute neurotoxicity of TOCP (triortho cresyl phosphate) of sciatic nerve in adult hen. *Journal of international academic research for multidisciplinary* 2015; 3: 2320-5083.
41. Liu P, Peng J, Han GH, Ding X, Wei S, Gao G, Huang K, Chang F, Wang Y. Role of macrophages in peripheral nerve injury and repair. *Neural Regen Res* 2019; 14: 1335-42.
42. Van Steenwinckel J, Auvynet C, Sapienza A, Reaux-Le Goazigo A, Combadiere C, Melik Parsadaniantz S. Stromal cell-derived CCL2 drives neuropathic pain states through myeloid cell infiltration in injured nerve. *Brain Behav Immun* 2015; 45: 198-210.
43. Cattin AL, Burden JJ, Van Emmenis L, Mackenzie FE, Hoving JJ, Garcia Calavia N, Guo Y, McLaughlin M, Rosenberg LH, Quereda V, Jamecna D, Napoli I, Parrinello S, Enver T, Ruhrberg C, Lloyd AC. Macrophage-Induced Blood Vessels Guide Schwann Cell-Mediated Regeneration of Peripheral Nerves. *Cell* 2015;162: 1127-39.
44. Chen P, Piao X, Bonaldo P. Role of macrophages in Wallerian degeneration and axonal regeneration after peripheral nerve injury. *Acta Neuropathol* 2015; 130:605-18.
45. Maiuolo J, Gliozi M, Musolino V, Carresi C, Nucera S, Macri R, Scicchitano M, Bosco F, Scarano F, Ruga S, Zito MC, Oppedisano F, Mollace R, Paone S, Palma E, Muscoli C, Mollace V. The role of endothelial dysfunction in peripheral blood nerve barrier: molecular mechanisms and pathophysiological implications. *Int J Mol Sci* 2019; 20: 3022.
46. Shimizu F, Sano Y, Abe MA, Maeda T, Ohtsuki S, Terasaki T, Kanda T. Peripheral nerve pericytes modify the blood-nerve barrier function and tight junctional molecules through the secretion of various soluble factors. *J Cell Physiol*. 2011; 226:255-66.

47. Sassoli C, Vallone L, Tani A, Chellini F, Nosi D, Zecchi-Orlandini S. Combined use of bone marrow-derived mesenchymal stromal cells (BM-MSCs) and platelet rich plasma (PRP) stimulates proliferation and differentiation of myoblasts in vitro: new therapeutic perspectives for skeletal muscle repair/regeneration. *Cell Tissue Res* 2018; 372:549–70.
48. Teymur H, Tiftikcioglu YO, Cavusoglu T, Tiftikcioglu BI, Erbas O, Yigitteurk G, Uyanikgil Y. Effect of platelet-rich plasma on reconstruction with nerve autografts. *The Kaohsiung journal of medical sciences* 2017; 33:69–77.
49. Chen NF, Sung CS, Wen ZH, Chen CH, Feng CW, Hung HC, Yang SN, Tsui KH, Chen WF. Therapeutic effect of platelet-rich plasma in rat spinal cord injuries. *Front Neurosci* 2018; 12:252.
50. Martinez CE, Smith PC, Palma Alvarado VA. The influence of platelet-derived products on angiogenesis and tissue repair: a concise update. *Front Physiol* 2015; 6: 290-9.
51. Soliman AF, Saif-Elnasr M, Abdel Fattah SM. Platelet-rich plasma ameliorates gamma radiation-induced nephrotoxicity via modulating oxidative stress and apoptosis. *Life Sci* 2019; 219: 238–47.
52. Zheng L, Ishii Y, Tokunaga A, Hamashima T, Shen J, Zhao QL, Ishizawa S, Fujimori T, Nabeshima Y, Mori H, Kondo T, Sasahara M. Neuroprotective effects of PDGF against oxidative stress and the signaling pathway involved. *J Neurosci Res* 2010; 88:1273-84.
53. Tong S, Zhang C, Liu J. Platelet-rich plasma exhibits beneficial effects for rheumatoid arthritis mice by suppressing inflammatory factors". *Molecular Medicine Reports* 2017; 16: 4082-8.
54. Zhang J, Middleton KK, Fu FH, Im HJ, Wang JH. HGF mediates the anti-inflammatory effects of PRP on injured tendons. *PLoS One* 2013; 8:e67303.
55. Abdul Ameer LA, Raheem ZJ, Abdulrazaq SS, Ali BG, Nasser MM, Khairi AWA. The anti-inflammatory effect of the platelet-rich plasma in the periodontal pocket. *Eur J Dent* 2018; 12: 528–31.
56. Guo SC, Tao SC, Yin WJ, Qi X, Yuan T, Zhang CQ. Exosomes derived from platelet-rich plasma promote the re-epithelialization of chronic cutaneous wounds via activation of YAP in a diabetic rat model. *Theranostics* 2017; 7: 81–96.
57. Huber HJ, Holvoet P. Exosomes: emerging roles in communication between blood cells and vascular tissues during atherosclerosis. *Curr Opin Lipidol* 2015; 26: 412-9.
58. Zheng C, Zhu Q, Liu X, Huang X, He C, Jiang L, Quan D. Effect of platelet-rich plasma (PRP)
- concentration on proliferation, neurotrophic function and migration of Schwann cells in vitro. *J Tissue Eng Regen Med* 2016; 10: 428-36.
59. Mammoto T, Chen Z, Jiang A, Jiang E, Ingber DE, Mammoto A. Acceleration of Lung Regeneration by Platelet-Rich Plasma Extract through the Low-Density Lipoprotein Receptor-Related Protein 5-Tie2 Pathway. *Am J Respir Cell Mol Biol* 2016; 54: 103–13.
60. Attia G, Atef H, Elmansi R. Autologous platelet rich plasma enhances satellite cells expression of MyoD and exerts angiogenic and antifibrotic effects in experimental rat model of traumatic skeletal muscle injury. *Egyptian Journal of Histology* 2017; 40: 443-58.
61. Carmeliet P, Jain RK. Molecular mechanisms and clinical applications of angiogenesis. *Nature* 2011; 473: 298–307.
62. Demidova-Rice TN, Wolf L, Deckenback J, Hamblin MR, Herman IM. Human platelet-rich plasma- and extracellular matrix-derived peptides promote impaired cutaneous wound healing in vivo. *PLoS One* 2012; 7: e32146.
63. Ruan GX, Kazlauskas A. Axl is essential for VEGF-A-dependent activation of PI3K/Akt. *EMBO J* 2012; 31:1692–703.
64. Kardas G, Daszyńska-Kardas A, Marynowski M, Brzakalska O, Kuna P and Panek M. Role of platelet-derived growth factor (PDGF) in asthma as an immunoregulatory factor mediating airway remodeling and possible pharmacological target. *Front Pharmacol* 2020; 11:47.
65. Moussa M, Lajeunesse D, Hilal G, El Atat O, Haykal G, Serhal R, Chalhoub A, Khalil C, Alaaeddine N. Platelet rich plasma (PRP) induces chondroprotection via increasing autophagy, anti-inflammatory markers, and decreasing apoptosis in human osteoarthritic cartilage. *Experimental cell research* 2017; 352: 146–56.
66. Bei Y, Wang F, Yang C, Xiao J. Telocytes in regenerative medicine. *J Cell Mol Med* 2015; 19:1441–54.
67. Marini M, Rosa I, Ibba-Manneschi L, Manetti M. Telocytes in skeletal, cardiac and smooth muscle interstitium: morphological and functional aspects. *Histol Histopathol*. 2018; 33: 1151-65.
68. Varga I, Polák Š, Kyselovič J, Kachlík D, Danišovič I, Klein M. Recently discovered interstitial cell population of telocytes: distinguishing facts from fiction regarding their role in the pathogenesis of diverse diseases called "telocytopathies". *Medicina (kaunas)*. 2019; 55:56.

-
69. Shahidi M, Vatanmakanian M, Arami MK, Sadeghi Shirazi F, Esmaeili N, Hydarporian S, Jafari S. A comparative study between platelet-rich plasma and platelet-poor plasma effects on angiogenesis. *Med Mol Morphol* 2018; 51:21-31.
 70. Kaux JF, Drion PV, Colige A, Pascon F, Libertiaux V, Hoffmann A, Janssen L, Heyers A, Nusgens BV, Le Goff C, Gothot A, Cescotto S, Defraigne JO, Rickert M, Crielaard JM. Effects of platelet-rich plasma (PRP) on the healing of Achilles tendons of rats. *Wound Repair Regen* 2012; 20:748-56.
 71. Miroshnychenko O, Chang WT, Dragoo JL. The Use of Platelet-Rich and Platelet-Poor Plasma to Enhance Differentiation of Skeletal Myoblasts: Implications for the Use of Autologous Blood Products for Muscle Regeneration. *Am J Sports Med* 2017; 45:945-53.
 72. Navani A, Li G, Chrystal J. Platelet Rich Plasma in Musculoskeletal Pathology: A Necessary Rescue or a Lost Cause? *Pain Physician* 2017; 20:E345-E56.
 73. Muth DC, Powell BH, Zhao Z, Witwer KW. miRNAs in platelet-poor blood plasma and purified RNA are highly stable: a confirmatory study. *BMC Res Notes* 2018; 273-81.
 74. Renn TY, Kao YH, Wang CC, Burnouf T. Anti-inflammatory effects of platelet biomaterials in a macrophage cellular model. *Vox Sang* 2015; 109:138-47.
 75. Saad Setta H, Elshahat A, Elsherbiny K, Massoud K, Safe I. Platelet-rich plasma versus platelet-poor plasma in the management of chronic diabetic foot ulcers: : a comparative study. *Int Wound J* 2011 8:307-12.
 76. Cáceres M, Martínez C, Martínez J, Smith PC. Effects of platelet-rich and -poor plasma on the reparative response of gingival fibroblasts. *Clin Oral Implants Res* 2012; 23:1104-11.

المُلْكُوكُ العَرَبِيُّ

دراسة هستولوجية على البلازم الفقيرة بالصفائح الدموية مقابل البلازم الغنية بالصفائح الدموية في تحسين الاعتلal العصبي السكري في الجرذان والدور المحتمل للخلايا الشبيهة بالخلايا ذات الامتدادات

داليا ابراهيم اسماعيل، إيمان عباس فرج

قسم الهيستولوجيا - كلية الطب - جامعة القاهرة

الخلفية: اعتلال الأعصاب السكري هو مضاعفة رئيسية مزمنة لمرض السكري، ويتميز بغيرات وظيفية وهيكيلية في الأعصاب الطرفية. البلازماغنية بالصفائح الدموية هي أحدى مشتقات الدم البيولوجية المشجعة التي اشتهرت وأثبتت فعاليتها في تطبيقات متنوعة.

الهدف من العمل: تقييم التأثير المحسّن المحتمل للبلازما الفقيرة بالصفائح الدموية مقابل البلازما الغنية بالصفائح الدموية على الاعتنال العصبي السكري المحدث في الجرذان.

المواد وطرق البحث: اشتملت هذه الدراسة على ثمان وأربعين من ذكور الجرذان البالغة البيضاء، عشرة للحصول على البلازما الغنية بالصفائح الدموية والبلازما الفقيرة بالصفائح الدموية. وتم تقسيم ثمان وثلاثين إلى أربع مجموعات: المجموعة الأولى (الضابطة). المجموعة الثانية (مجموععة اعتلال الأعصاب السكري): تلقت حقنة واحدة داخل الغشاء البريتوني من STZ (٦٠ ملجم / كجم) وتركت حتى نهاية التجربة. بعد ٦٠ يوماً من مرض السكري تلقت المجموعات الثلاثة (مجموععة البلازما الغنية بالصفائح الدموية) والرابعة (مجموععة البلازما الفقيرة بالصفائح الدموية) ٥،٥ مل / كجم من البلازما الغنية بالصفائح الدموية أو البلازما الفقيرة بالصفائح الدموية تحت الجلد مرتين أسبوعياً لمدة ٣ أسابيع. تم تقييم وزن الجسم، وجلوکوز الدم، وسرعة التوصيل العصبي وmiRNA 146a ، وكذلك تم قياس MDA، وTNF α ، NGF، وZO-1 و claudin 1 بالأنسجة. تمأخذ عينات العصب الوركي الأيمن ومعالجتها للصباغة بالهيماتوكسيلين والإيوسين ، والتوليدين الأزرق ، والصباغة الهستوكميائية المناعية ضد CD34، S100 و3-aspase وCD34، تم صباغتها للميكروскоп الإلكتروني. تم قياس عدد الخلايا المناعية الإيجابية لـ CD34، والمساحة المئوية لرد الفعل المناعي لـ caspase-3 ، بالإضافة إلى نسبة-G والمساحة التجويفية للشعيرات الدموية. وأتبع ذلك بالتحليل الإحصائي.

النتائج: أظهرت مجموعة اعتلال الأعصاب السكري تغيرات كيميائية حيوية ونسوجية: كاعتلال الأعصاب، واعتلال خلايا شوان واعتلال الأوعية الدموية مع تأثير سرعة التوصيل العصبي والخلايا الشبيهة بالخلايا ذات الإمتدادات. أظهرت مجموعة عادي البلازما الغنية بالصفائح الدموية والبلازما الفقيرة بالصفائح الدموية نتائج مماثلة لبعضها والمجموعة الضابطة. فقد أظهرتا سمات كيميائية حيوية ونسوجية وسرعة توصيل عصبية طبيعية تقريبا. كما أظهرت كلتا هما زيادة ملحوظة في التعبير المناعي لـ S100 وCD34 مع انخفاض كبير في المساحة المئوية لـ caspase-3 مقابل مجموعة اعتلال الأعصاب السكري.

الاستنتاج: أثبتت البلازما الفقيرة بالصفائح الدموية والبلازما الغنية بالصفائح الدموية تأثيراً تحسينياً على اعتلال الأعصاب السكري من خلال تحسين التغييرات الكيميائية الحيوية والنسيجية والحفاظ على الخلايا الشبيهة بالخلايا ذات الامتدادات.